國　立　交　通　大　學

奈 米 科 技 研 究 所

碩 士 論 文

新穎背向閘極奈米線場效電晶體結合自組裝單分子層於即時偵測肝癌生物標記感測器之應用與探討

Real-Time and Label-Free Detection of the Cancer Maker of Hepatocyte Tumor by a Novel Back-gated SiNB-FET Biosensor.

研究生：李柏軒　　**Bo-Syuan Lee**

學號：　9652509

指導教授：柯富祥 博士　　**Dr. Fu-Hsiang Ko**

中華民國九十八年 7 月

新穎背向閘極奈米帶場效電晶體結合自組裝單分子層於

即時偵測肝癌生物標記感測器之應用與探討

Real-Time and Label-Free Detection of the Cancer Maker of Hepatocyte Tumor by a Novel Back-gated SiNB-FET Biosensor.

研究生: 李柏軒　　Bo-Syuan Lee

指導教授: 柯富祥 博士　　Dr. Fu-Hsiang Ko

國立交通大學

奈米科技研究所

碩士論文

A Thesis
Submitted to Institute of Nanotecnology
College of Engineering
National Chiao Tung University
in Partial Fulfillment of the Requirements
for the degree of
Master in
Nanotechnology
July 2009
Hsinchu, Taiwan, Republic of China

中華民國九十八年７月

Acknowledgment

這兩年的碩班生活，首先要感謝的當然是柯富祥博士。因為柯老師總是會為學生著想，也總是支持著學生的理想，學術上對我提供的幫助自然更不在話下。這段時間能讓我在專業領域與待人處事上跨進一大步，是因為有老師您。

再來，要感謝其昌學長在實驗上實質與精神上的幫忙！這兩年來，謝謝你提供不管是在元件上，或知識上的支援，真不敢想像如果沒有你在，我的碩士論文會是甚麼模樣。我超崇拜你的，你是真男人！再來我想要謝謝中書學長，嘖嘖，實驗室生物相關的問題我好像只能問同背景的你，也謝謝你熱心的跟我討論，還無私的教我奈米金的製備與應用，雖然最後好像都沒用到哈哈哈。我也感謝一開始帶我實驗的皮皮學姊，謝謝妳一開始給我的啟蒙，不然我還真不知實驗要從哪做起。再謝謝桃子學姐，之前我碩一甚麼都不懂所以問了很多蠢問題，不過你還是有問必答，實在是非常的有耐心。謝謝強者我同學林京璋，除了偶爾跟你討論實驗獲得的寶貴靈感外，最重要的是我們在某大型多人３Ｄ立體技術交流平台上一起奮鬥的日子，諸如團隊合作，與責任感，我想我學到了很多，祝你早生貴子。謝謝鄭捷，一個曖曖內含光的帥哥，謝謝你提供實驗室區域連線多媒體，讓實驗室隨時都充滿著挑戰與歡樂，而且還開車帶我們環校觀光，吃晚餐。謝謝一點都不像雙子座的馮玟菲，謝謝妳提供的肝細胞，我也一直很欣賞妳的行事風格，哈。謝謝何嘉琦，祝妳減肥成功，雖然你一點都不胖阿。。。實驗與論文方面，我相信妳一定沒問題啦，絕對可以早早畢業！蘇丁香，謝謝你在實驗上給我的支持與幫助，現在想想，如果沒有妳提供的笑點，在實驗不順利時其實是非常的悶阿！還有加油喔，很遺憾畢業後在實驗方面沒辦法繼續支持妳，不過我知道妳一定行的，明年就換妳畢業了。佳典學長，你講的笑話我一直都覺得很好笑，哈。小朱學長，謝謝你不厭其煩的幫我設定機台，和解決一些實驗室的疑難雜症。品麟學長，還記得我們在ＮＤＬ奮鬥的日子嗎？那段時間你也教導了我許多機台相關的知識。貞治同學，雖然我們有時候會搶機台，不過我也要感謝你在ＮＤＬ陪我做實驗，和幫我訂便當ＸＤ。當然還要謝謝實驗室其他在不同領域中共同努力及患難與共的夥伴們：俊淇學長，３.com 學長，Jagon 學長，宜生學長，美榕學姐，易成（一直跟我借刷子），懷箴，崇志，品樺。因為有你們，讓我碩士生活平添了許多色彩。

最後我要感謝我的父母，兄弟姊妹，這兩年來給我的關心與包容，讓我能隨時準備好面對挑戰。家住在台南，在新竹讀書卻沒能常常回家實在非常汗顏。我會再持續進步，直到我有能力讓你們過著更好的生活，報答你們的養育與教導之恩。。。

謹以此文　獻給我身邊的你們

新穎背向閘極奈米帶場效電晶體結合自組裝單分子層於即時偵測肝癌生物標記感測器之應用與探討

學生：李柏軒　　指導教授：柯富祥 教授

國立交通大學奈米科技研究所碩士班

摘 要

場效電晶體元件與生物分子偵測的連結應用在未來的疾病診斷與防治是個重要且具發展淺力的新興科技。在此篇論文中，我們選擇血液酸鹼值，B 型肝炎病毒 X 基因的去氧核醣核酸(DNA)片段序列與甲型胎兒蛋白(alpha feto-protein)抗原來當作偵測肝炎，肝硬化，與肝腫瘤的指標。我們以奈米米帶場效電晶體(nanobelt field effect transsitor)為元件基礎的裝置，做為即時偵測、不需外加標定、高靈敏度以及高特異性結合的生物感測器，可偵測的生物分子或是化學物種包括有低濃度化學成分離子、小分子、抗原抗體反應、去氧核醣核酸片段與檢測蛋白質。在我們的研究裡，使用了互補式金氧半場效電晶體的技術來製作新穎背向閘極奈米帶場效電晶體生物感測器。利用矽的局部氧化製程(LOCOS)來製作內縮線寬的奈米帶，而此奈米帶可以達到優異的高比表面積比以及獲得背向閘極控制，此兩項主要特色對於目前感測元件整合於微流道組件上有極大優勢及應用面潛力。我們量測血液酸鹼值、B 型肝炎病毒 X 基因的去氧核醣核酸片段序列以及癌症指標物甲型胎兒蛋白抗原對於場效奈米帶

元件的電性變化影響，另外還利用了原子力顯微鏡、螢光顯微鏡以及電子顯微鏡量測儀確認表面自組裝固定化的技術以及生物分子實驗條件的確立。

最後總結出我們利用矽的局部氧化製程製作出的奈米帶通道可使其線寬內縮到 150 奈米以下的線寬，此條件提供元件電性達到優異的 10^5 倍的開關電流比。利用此靈敏度高的元件我們可以偵測到接近濃度 1fM 的標的突變 DNA 以及濃度為 3ng/mL(? 最靈敏應可作到很低)的癌症標誌物抗原分子。結果顯示此新穎的背向閘極奈米線感測元件可以用作未來的免標定、即時偵測、高靈敏度以及優異專一性結合的場效奈米帶電晶體生物感測器。另外，此元件具有控制背向閘極的能力更提供了未來感測元件與微流道技術整合上的一大優勢。

Real-Time and Label-Free Detection of the Cancer Maker of Hepatocyte Tumor by a Novel Back-gated SiNB-FET Biosensor.

Student: Bo-Syuan Lee **Advisor: Prof. Fu-Hsiang Ko**

Institute of Nanotechnology

National Chiao Tung University

Hsinchu 300, Taiwan, ROC

Abstract

The application of high-sensitive field-effect transistor devices in detecting the biomolecules is an important and developing thchnology. The development of biological sensors could ımpact significantly the areas of genomics, proteomics, biomedical diagnostics, and drug discovery in the future. In our thesis, the serum pH value, HBV X gene DNA fragments, and α-fetoprotein cancer marker were chosen as the target molecules to detect the hepatocellular carcinoma. The devices based on semiconducter nanobelt exhibited highly sensitive and selective characteristics for the real-time, label-free, and excellent specificity detection of biomolecules and chemical species. A novel back-gate silicon nanobelt field effect transistor (SiNB-FET) was fabricated by using the complementary metal oxide semiconductor (CMOS) compatible technology. The shrank nanobelt with high surface-to-volume ratio and individual back-gate were achieved by the local-oxidation of silicon (LOCOS) process. Because of the above advantages, the devices have potential to integrate with microfluidic system for bio-detection application. Therefore, the detection of hepatocellular carcinoma was investigated by measuring the characteristics of electrical signals. The atomic force microscopy (AFM)、fluorescence microscopy and scanning electron microscopy (SEM) were also examined to check out the self-assembly efficiency and appropriate experimental parameter for bio-sensing.

In conclusion, the width of nanobelt by LOCOS process can be shrank down to 150 nm. The drain current versus gate voltage (I_d-V_g) characteristic of the

SiNB-FET exhibited about five orders of magnitude of I_{on}/I_{off} current ratio, and the threshold voltage shifts positively after hybridization of 1fM concentrations of HBV X gene DNA fragments and 3ng/mL concentrations of the cancer marker, antigen-α-AFP, respectively. The results show that the back-gated nanobelt device has the capability of acting as a real-time, label-free, highly sensitivity and excellent selectivity SiNB-FET biosensor in detecting biomolecules. Our approach offers the possibility of highly potential to integrate microfluidic-channel system for future parallel real-time detection of multiple chemical and biological species with controlling the individual back-gate in a single integrated chip.

Content

List of Figures

Chapter 1: Introduction

Chapter 2: Paper review

Chapter 3: Experimental procedure

Chapter 4: Result and Discussion

Chapter 1: Introduction

1.1 General introduction

Nanotechnology, which is sometimes shortened to "Nanotech", refers to a region whose study is the control of matter on an atomic and molecular scale. Nanotechnology is also believed that is a important revolution about science, industry, and our life. A nanometer is one-billionth of a meter. A sheet of paper is about 100,000 nanometers thick; a single hydrogen atom is about a 1/10 nanometer in diameter. Nanoscale means something diameter is about 1 to 100 nanometers. Under the nanoscale level, different physical, chemical, and biological properties could emerge. These properties may bring the diverse important application way from the properties of bulk materials and single atoms or molecules.

Generally, nanotechnology is definition as a skill that to handles structures of the size 100 nanometers or smaller, study and technology development at the atomic, molecular or macromolecular scales, to provide a fundamental understanding of phenomena and materials at the nanoscale and to create and applied structures, devices and systems that have novel properties and functions because of their small and/or intermediate size.

The first use of the concepts in 'nano-technology' (but predating use of that name) was in "There's Plenty of Room at the Bottom," a talk given by physicist Richard Feynman at an American Physical Society meeting at Caltech on December 29, 1959. The benifit of nanotechnology is rooted in its potential to transform and revo-

lutionize multiple technology and industry sectors, including aerospace, agriculture, biotechnology, homeland security and national defense, energy, environmental improvement, information technology, medicine, and transportation.

Nanotechnology is going to change the world and the way we live, creating new scientific applications that are smaller, faster, stronger, safer and more reliable.

Figure 1 is the diagram of nanotechnology, the nanotechnology is belong in the mesososmic region, in this size many material will result somewhat new property, Created and applied structures, devices and systems that have novel properties and functions cause by their small and/or intermediate size.

Fig. 1-1 Diagram of nanotechnology. Nanotechnology is technology development at the atomic, molecular or macromolecular scales. Created and applied structures,

devices and systems that have novel properties and functions cause by their small and/or intermediate size.

1.2 Top-down and bottom-up

There are two groups of researcher with opposing approaches to nanotechnology utilization will meet and find a middle ground. The two camps are informally referred to as "top-down" and "bottom-up"[1]. Top-down methods start with patterns made on a large scale and reduce its lateral dimensions before forming nanostructures. On the other hand, bottom-up methods begin with atoms or molecules to build to nanostructures, in some cases through smart use of self-organization. The bottom-up researchers attempt to build nanodevices one molecule at a time, rather like the way that living organisms synthesize macromolecules [2].

1.2.1 Top-down method

Top-down methods for nanopatterns can be subdivided into bulk-/ film-machining, surface-machining, and soft lithography (Fig. 1-2). In bulk-/film-machining the channel is created by etching trenches in the substrate wafer or, alternatively, in the film deposited on the substrate. This is done typically by conventional photolithography followed by wet or dry etching of the substrate [3, 4]; In surface-machining[4, 5], first a bottom layer is deposited on the wafer followed by the deposition of the sacrificial layer and its patterning . Then, the top layer is deposited on top of the sacrificial layer and patterned (often with irrigation holes, which provide the access to the sacrificial layer). The nanochannel is finally formed by removing, i.e., etching the sacrificial layer leaving the bottom and the top layer to

form the walls of the nanochannel. In soft lithography, the mold in the inverse shape of the desired structure is formed. This is filled with a structural material and then the mold can be etched or removed leaving the desired structure behind [1]

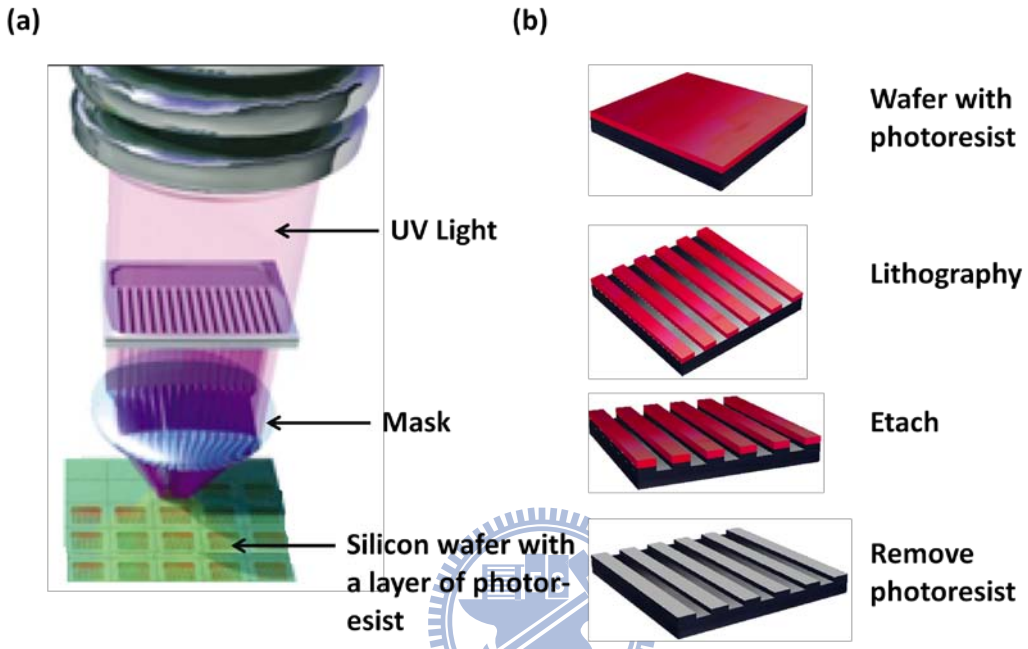

Fig.1-2 Schematic diagram of the top-down method. (a) Conventional photolithography procedure. This procedure separates into two stages, stage one is preparation the mask, and stage2 is applied the mask to manufacture replicas. (b) A typical bulk-/ film-machining. The channel is created by etching trenches in the substrate wafer or, alternatively, in the film deposited on the substrate.

1.2.2 Bottom-up methods

In bottom-up methods, the atoms and molecules are assembled into the smallest nanostructures (typically dimensions is from 2 to 10 nm) by carefully controlled chemical reactions (Fig. 1-3), which make this technique cheaper as compared to the lithographical methods.

Self-assembly of atoms and molecules into nanostructures can be classified as a bottom-up method. In nature, self-assembly is often used to make complex structures. At present, the mastery of self-assembly is limited to relatively simple systems. To achieve complex systems hierarchical self-assembly can assist, where the products of one self-assembly step is a base for the next one. The formation of self-assembled monolayers (SAMs), that are produced when a substance spontaneously forms a molecular monolayer on a surface, could be successfully combined with standard lithographical methods to achieve large-scale and better controlled structures [1].

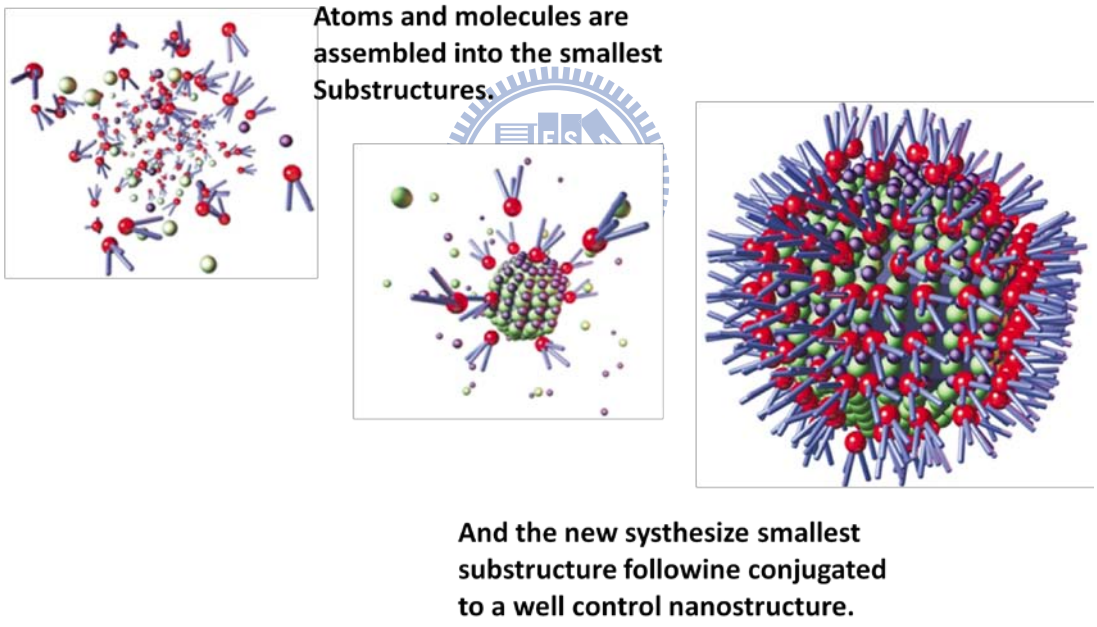

Fig. 1-3 Diagram of bottom up procedure. A chemical reaction brings together some molecules aggregate to small crystal, and the small crystals attract surroundings into a nanopartical.

In summary, Top-down methods are based on patterning on large scale while reducing the lateral dimensions to the nanoscale. Bottom-up methods arrange atoms

and molecules in nanostructures. Although the two methods seem to depend on opposite strategies, they are not repelled. A promising approach is the combination of both top-down and bottom-up methods, where the smallest nanostructures achieved by bottom-up methods can be controlled and interconnected by previously employed lithographical methods. For example, the ref [6], and [7], a study in description of CNTs grown by the CVD technique within anodic aluminum oxide nanopore arrays (AAO). In this way, excellent uniformity in the size and disposition of nanotubes was achieved as well as naturally perpendicular growth to the rigid substrate without a need for an extra processing step.

1.3 Employment of bioFET for ultra sensitive sensing

The world we live are full of numerous invisible particles, including different kinds of chemical compounds, DNA, RNA, proteins, virus, bacteria, and germs. Parts of these invisible particles are good for us, something indeed cause us feel disorder ever and let us get disease; , the others play the role of reporter, send us several significant message from our inner body, or outer different kind of invader [8].

There were various researches in detecting the above particles by using optical, spectrometric, electrochemical, or SPR methods. However, all of these methods, unfortunately, have drawbacks of time-consuming, fail sensitive, less selective, and multi-stage processes that are expensive and unsuitable for on-line monitoring.[9]. Recently, many papers have proposed the biosensor based upon semiconductor field effect transistor (FET) demonstrated ultrahigh sensitive performance [10-13]. FET is a type of transistor that relies on an electric field to control the conductivity of channel by modulating the charge carrier in a semiconductor material. BioFET

combines the FET and some particular biomolecular like DNA or protein, utilize the characterize of FET and the specific recognized binding force of biomolecular to sense and detect the desired target molecular [15] .

Because of the mature fabrication process of FET,the it is easy to get standardization , miniaturization, mass production, and global intergradations. The novel device sensor can be associated the application with to extend field, in such fields as medical diagnostics, biological research, environmental protection, and food analysis.

The most important step in fabricating the bioFET sensor is the function of the molecules which bear the select captured ability to bind target molecular o sense on the gate oxide surface. The immobilized layers, named 'SAM', are meant self-assembled monolayer. A self assembled monolayer (SAM) is a regular layer of aliphatic compound in which one end of the molecule, the "head group" own a special affinity or covalence bonding capability for a substrate face, in our case, a silicon oxide surface. SAMs also consist of a tail with a functional group at the terminal end, which we can employ to link another molecular, generally, a bio sensing molecular. Areas of close-packed molecules nucleate and grow until the surface of the substrate is covered in a single monolayer[15]. The SAM we immobilized is able to capture chemical compound, DNA, and protein we interest. In this paper, we will use some different SAM such as ssDNA and anti-body for the desire of detection different gene and antigen.

In a conventional field effect transistor, the drain current is dependant to the gate potential. In bio-FET, it is expected that the drain current varies due to the existence of protein and DNA functionalized on the gate. A charged molecule bound onto an NB surface exerts an electric field in a manner similar to an applied gate voltage. For example, when the surface receptor contains a macromolecule of DNA bearing negative charge, specific binding interactions will result in an increase in the NB's

negative charge, and, hence, a shift to the right for the I_D–V_G curve of the NBFET biosensor. Therefore, the target molecular with a charged carrying could be detected by this BioFET.

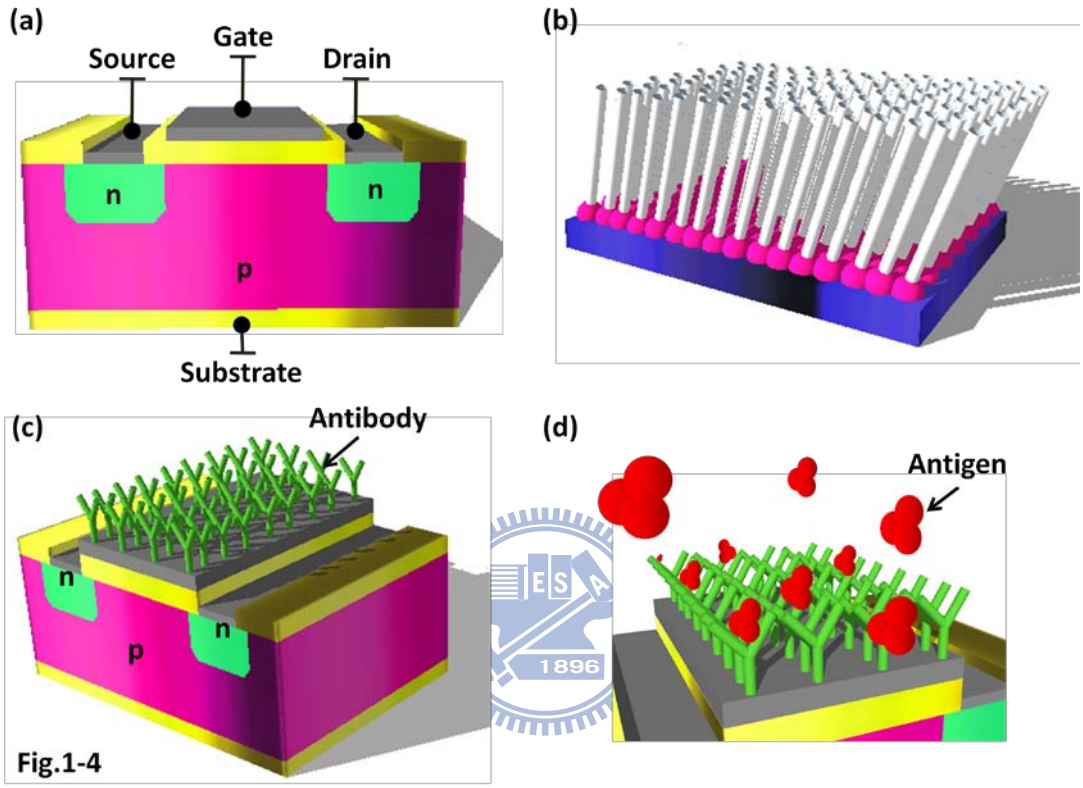

Fig. 1-4 Diagram of biosensor. (a) A typical field-effect transistor, containing source, drain and gate. Fig.1-4(b) A self assembled monolayer (SAM) is a regular layer of aliphatic compound in which one end of the molecule. Fig.1-4(c) BioFET is combine the FET and some particular biomolecular like DNA or protein for sensitivity and specific sensing. Fig1-4(d) Sensitive and specific recognized binding force between capture molecular (ex: antibody) and target (ex: antigen).

1.4 Utilize the bioFET to diagnosis hepatocellular carcinoma (HCC)

Hepatcellular carcinoma is one of the most malignant tumors of all cancer, especially in Taiwan. According to the department of health, HCC is the top one death reason for male and the second death reason for female. HCC generally break out in the time of our summer of life. And because the liver has few nerve system spread, it is general late when we have vigilance from own liver. And base on the statistics, if we only rely on the sensitive of the traditional diagnosis system of HCC, the prognosis is general not good, the average last time is only six to nine months. As the reason, if we got cancer, it absolute is a big cost no matter for our self, our family, or our society. For these reason, early detection HCC disease is very important for us. We chose the (1) blood pH, (2) the blood AFP (AFP), (3) and the blood HBV DNA as the examining target.

1.4.1 Detection the blood pH value

When our liver has a little pathological change, the liver cell may transform, the transform liver cell has much actively metabolism, this cause more CO_2 diffusion to blood, and the abnormal liver cell also produce more acidic poison protein, these two elements will decrease the pH of the blood away pH 7.4.

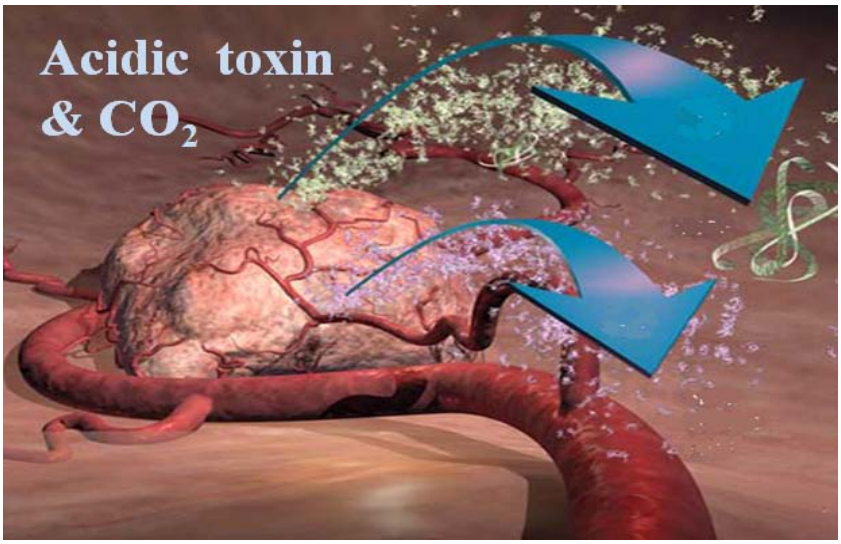

Fig.1-5 Secretion of the abnormal liver tumor. Transform liver cell or hepatocyte tumor metabolism much activity, caused more and more CO_2 diffusion to blood, and the abnormal liver cell (ex: hepatocyte tumor) also produce excess acidic poison protein (ex: AFP), these two elements will cause metabolic acidosis.

1.4.2 Detection the blood alpha-fetoprotein (AFP)

Alpha-fetoprotein (AFP, α-fetoprotein) is a protein [17][18] which in humans is encoded by the *afp gene*[19][20]. AFP is produced dominant by liver. Once our liver has damage the AFP produced by liver will leak out to the blood vessel, caused the blood AFP concentration increased. Published reports indicate that AFP (AFP), expression in adults is often associated with hepatoma or teratoma. Like any elevated tumor marker, elevated AFP by itself is not diagnostic, only suggestive. The AFP concentration is one of the most important indexes of the liver physical condition. A good parts of health examination nowadays also test the concentration of AFP for liver function determine.

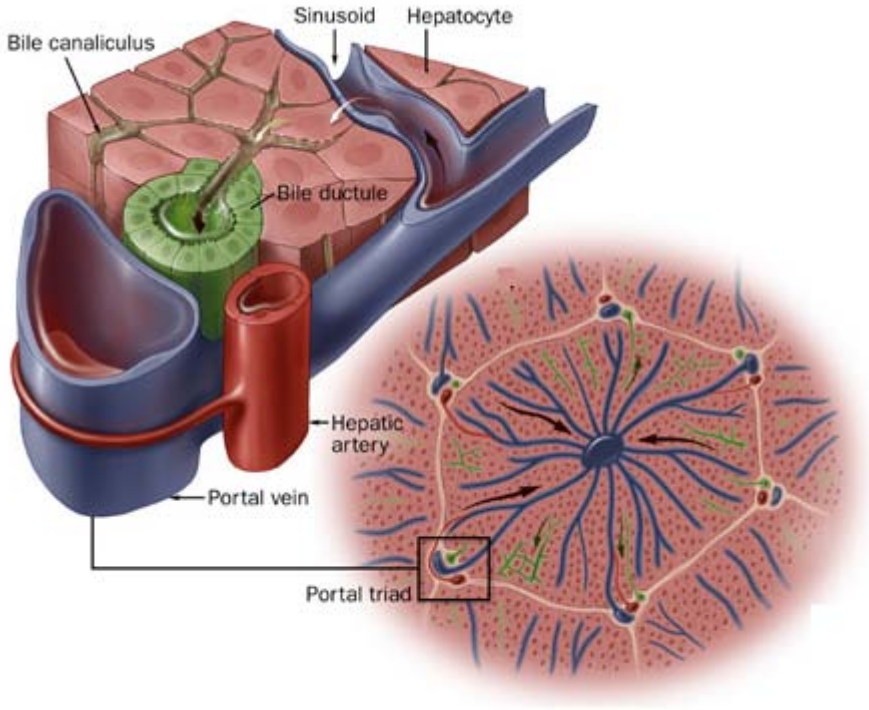

Fig.1-6 AFP secretion by abnormal liver. Alpha-fetoprotein (AFP, α-fetoprotein) which in humans is encoded by the *afp gene* is produced dominant by liver. Published reports indicate that AFP, excess expression in adults is often associated with hepatoma or teratoma.

1.4.3 Detection the blood HBV X gene DNA fragments

HBV infection data and history of chronic hepatitis disease were provided by the doctors in primary care centers according to earlier examinations and records. The serum HBV marker (anti-gens and antibodies of HBV) had been checked in most of recruited subjects before the study started. Most people now agree that screening for PLC in groups with HBV infection or with liver cirrhosis does detect PLC at an early stage [21]. Therefore, we plan use the HBV serum DNA as a cancer maker as HCC. The X gene of HBV seems to play an important role in HBV-associated hepatocarcinogenesis[22]. The human hepatitis B virus X gene encode a 17 KDa pro-

tein, named X, which is known to associated in insulin-like growth factor-II synthesized [6] (fig.1-7). In the physical pathway, insulin-like growth factor-II (IGF-II) is believed to function as a trigger for cell transformation, and malignant of hepatocyte tumor by autocrine or paracrine mechanisms (Fig. 1-8). X protein also complexes with the ~53 protein and inhibits its sequence specific DNA binding, transactivating and apoptotic capacity[22]. The *p53* protein is a prototype tumor suppressor gene that is well suited for analysis of mutational spectrum in human cancer, it is the most common genetic lesion in human cancers, HBV X protein complexes with the *p53* protein and inhibits its sequence specific DNA binding, transactivating and apoptotic capacity. (Fig. 1-9)

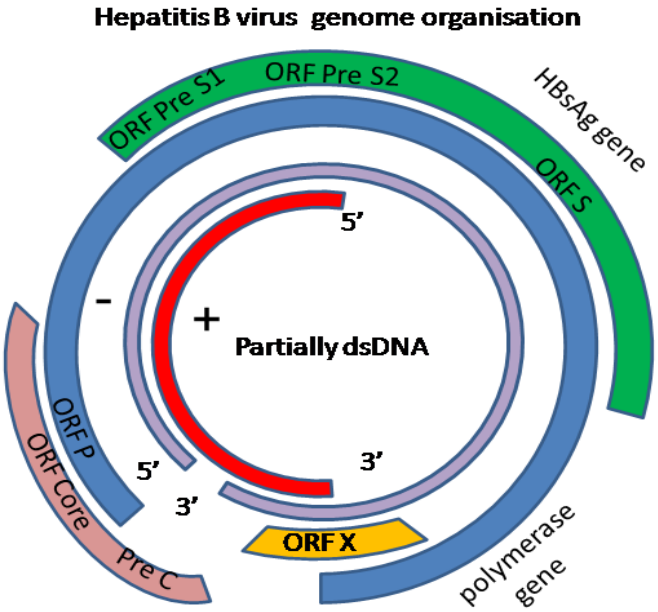

Fig. 1-7 Genome of human Hepatitis B Virus. Hepatitis B virus encode a 17 KDa protein, named X, which is known to associated in insulin-like growth factor-II synthesized.

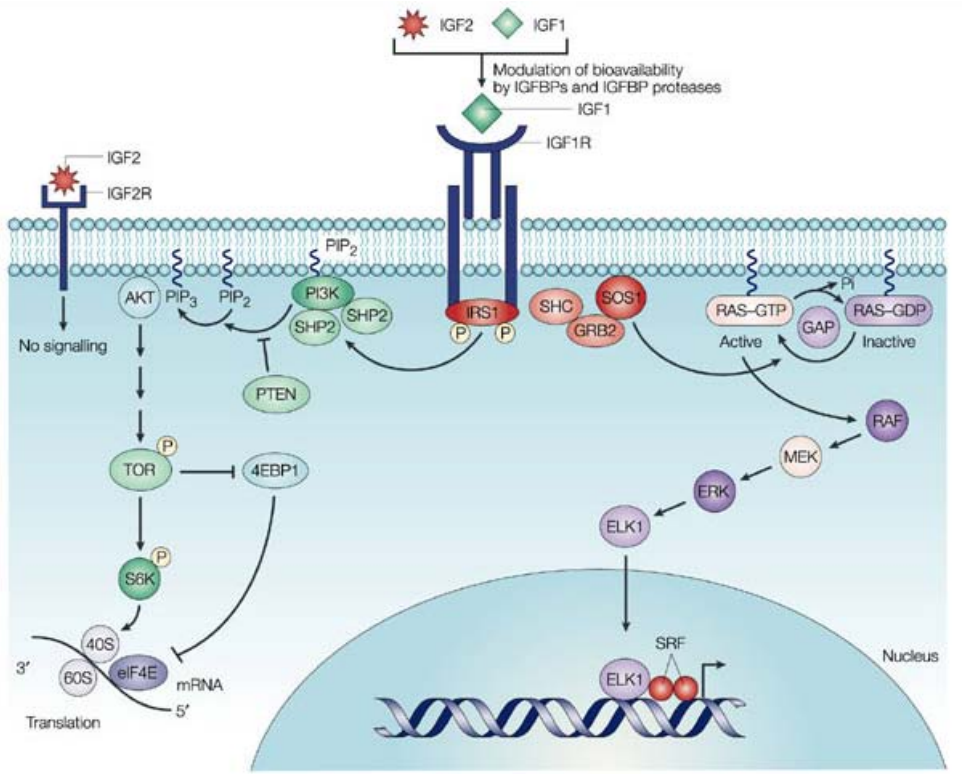

Fig 1-8 IGF-II physiology pathway. Insulin-like growth factor-II (IGF-II) is believed to function as a trigger for cell transformation, and malignant of hepatocyte tumor by autocrine or paracrine mechanisms. (*Figure source: Nat Rev Cancer@2004 Nature Publishing Group*)

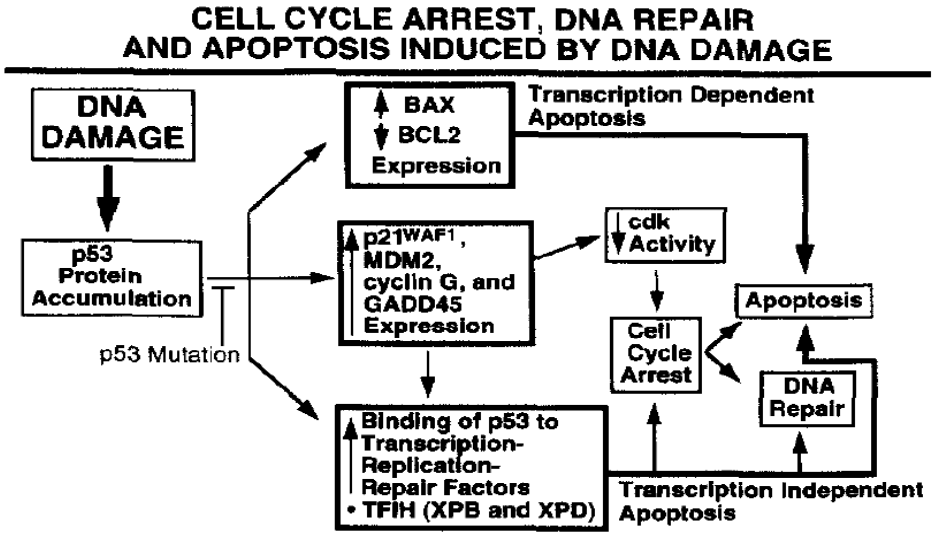

Fig. 1-9 *p53* physiology path way. *p53* is a prototype tumor suppressor gene, it is

the most common genetic lesion in human cancers, HBV X protein complexes with the p53 protein and inhibits its sequence specific DNA binding, transactivating and apoptotic capacity.

To summarize, HCC is one of the commonest malignancies in Asia. Clinical studies have shown that only if HCC is detected at a presymptomatic stage can it be surgically resected with even the possibility of a cure. However, since HCC is usually associated with liver cirrhosis and there is often intrahepatic metastasis[21], surgical resection is suitable only for patients at an early stage of the disease. This means that early detection is the key of human to fight with HCC.

Chapter 2: Paper review

There are numerous important elements to alter the lift-time, stability, selectivity, and sensitivity of BioFET type sensor. The self-assemble monolayer functioned on the gate oxide is one of the most important element. The surface concentration, cloudy aggregation, duration, and crystalation of SAM will strongly influence the performance of sensor. Except the property of SAM, the concentration, temperature, pH, and ion contain also play a major role on capture ability, sensitivity, and selectivity of sensor. Fortunately, there are many research group have studied this region in the whole world, therefore, the paper which reported these subject is also abundant, following we will cite the literatures which we think are representative which we had reviewed (paper about SAN and buffer properties we will divided into two part). Naturally, and certainly the application of a BioFET is also important and interest for consider, so we also present some literature we have reviewed at the last part.

2.1 Literature about self-assembled monolayer

Aminated silane films are currently used in a wide variety of both industrial and research-oriented applications. Specifically, 3-aminopropyltriethoxysilane (APTES) is a commonly used coupling agent for the modification of silica surfaces to increase hydrophilic properties[1-4]. APTES is also used in attaching metal nanoparticles to silica substrates because of the strong interaction between the amine group and the metal particles[5][6]. APTES films are also used to promote protein adhesion for biological implants and in lab-on-a-chip applications[13-15]. While many studies focus on the characterization of APTES[14-22], or other alkoxysilane films, most are limited in scope, focusing on single reaction variables or a narrow set of deposition

conditions without offering a clear, comprehensive guide to the best method of film formation. As a result, there is a wide range of reaction conditions used to deposit APTES films. Hydrolysis of silane drives the attachment of the APTES to the substrate resulting in siloxane bonds at the substrate surface. Basic functional groups such as amines will self-catalyze the hydrolysis reaction leading to more aggressive monolayer formation as compared to nonaminated silanes[24]. The initial hydrolysis step can occur either in solution or at the substrate surface depending on the amount of water present in the system. An overabundance of water will result in excessive polymerization in the solvent phase, while a deficiency of water will result in the formation of an incomplete monolayer[25]. APTES films are subject to disorder, even as a monolayer, as it is possible for the amines to hydrogen bond to the substrate or for the entire molecule to bend such that the head-and-tail groups are oriented toward the substrate surface[24]. Solvent, concentration, reaction time, and reaction temperature also have an effect on the attachment kinetics. Incomplete coverage of the surface by APTES can be equally problematic. Understanding the mechanisms and kinetics of the monolayer formation is critical to creating well-controlled surfaces. The aim of this work is to establish the optimum reaction conditions for preparing uniform thin films of APTES on silica. The ideal film in this system will have maximum surface coverage of amine functional groups and surface roughness on the order of the underlying substrate. AFM tapping mode scans are summarized as 3 X 3 grids in Fig.2-1. Each plane has nine separate surfaces all with the same reaction temperature (75 °C on top and 25 °C on bottom). APTES concentration is presented along the x-axis, reaction time along the y-axis, and reaction temperature along the z-axis.

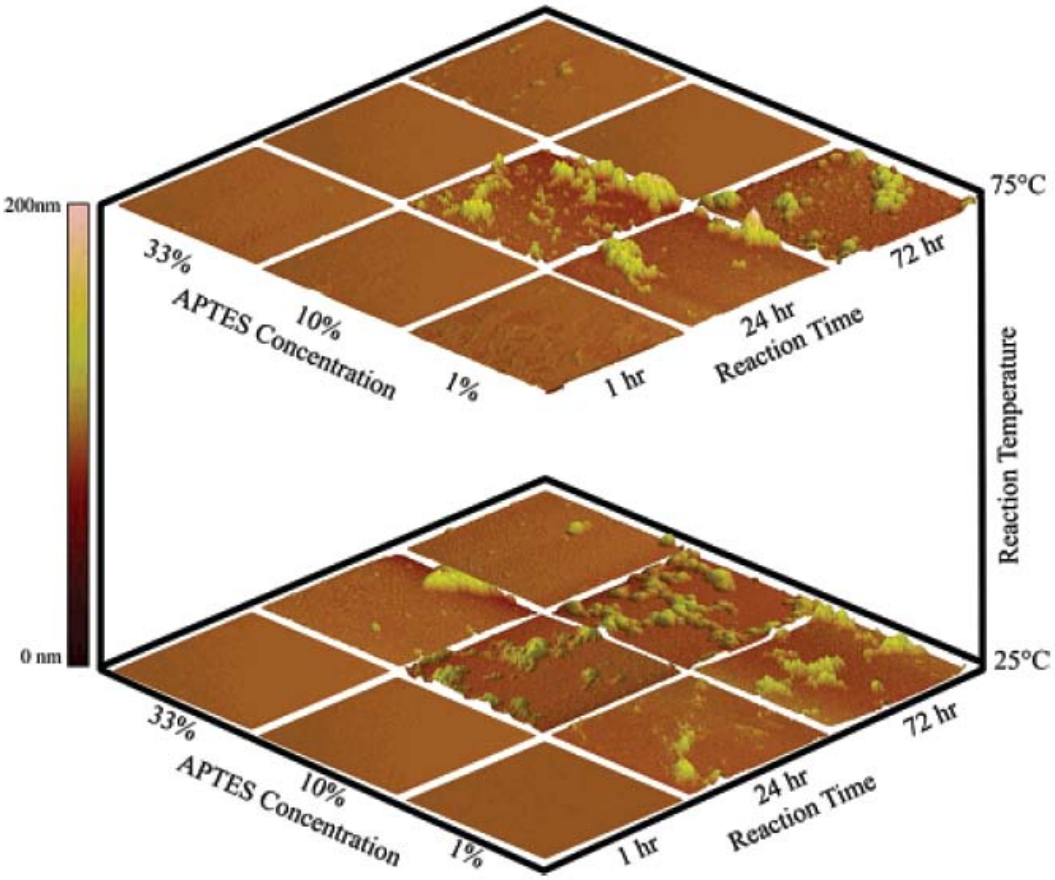

Fig. 2-1 APTES films scan by three-by-three matrix AFM. Each individual image is 2 um X 2 um with a height scale of 200 nm (displayed left).

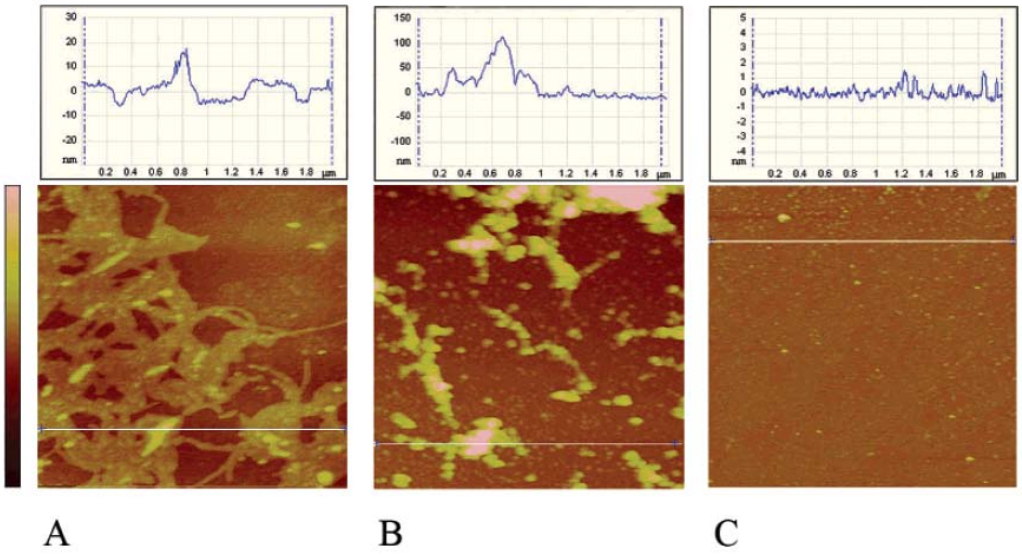

Fig. 2-2 Representative morphologies of APTES films. (A) Multilayer-island growth on top of a complete film deposited at 1%-1 h-75 °C, height scale is 30 nm.

(B) Rough APTES film deposited at 10%-24 h-75 °C, height scale is 150 nm. (C) Smooth APTES film deposited at 33%-24 h-75 °C, height scale is 10 nm. Horizontal lines indicate profile views.

Increasing the concentration of the APTES solution for films deposited at 75 °C resulted in decreasing the RMS roughness for 24- and 72-h reactions (and it had a negligible effect for 1-h reactions). For the 24-h reaction, this effect was realized only for the 33% solution, whereas the 72-h reaction resulted in an RMS decrease for both 10% and 33% solutions compared to 1% APTES solution. These three films deposited at 75 °C were smoother than their 25 °C counterparts. Ellipsometry was used to determine the thickness of the APTES films; the resulting data are presented graphically in Figure 2-3.

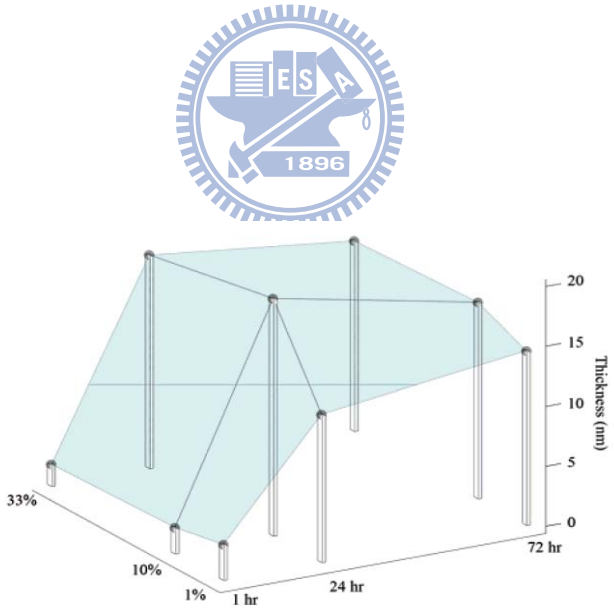

Fig. 2-3 Ellipsometry data as a function of reaction. The experimental conditions was 75 °C reaction temperature (left) and 25 °C reaction temperature (right).

When comparing samples at various APTES concentrations or temperatures when the APTES reaction is limited to 1 h, some important differences were apparent.

These interested phenomenons would be due to APTES hydrolysis can occur most efficiently and completely if there is sufficient surface water available for the reaction. The first monolayer of APTES reacts with a hydrated surface as shown in Figure 2-4 similar to the mechanism of deposition of trichlorosilanes[26][27]. As this reaction proceeds and a continuous film is formed, water is no longer concentrated at the film surface but is primarily in solution. As APTES concentration increases, it becomes more likely that water in the system will react with an unreacted APTES molecule as opposed to further hydrolyzing APTES molecules already deposited in the film. Thus, the APTES molecules deposited from a high APTES solution concentration are quickly buried before they can fully hydrolyze. As surface water is used up, the deposited APTES can no longer attain high degrees of hydrolysis in the substrate surface.

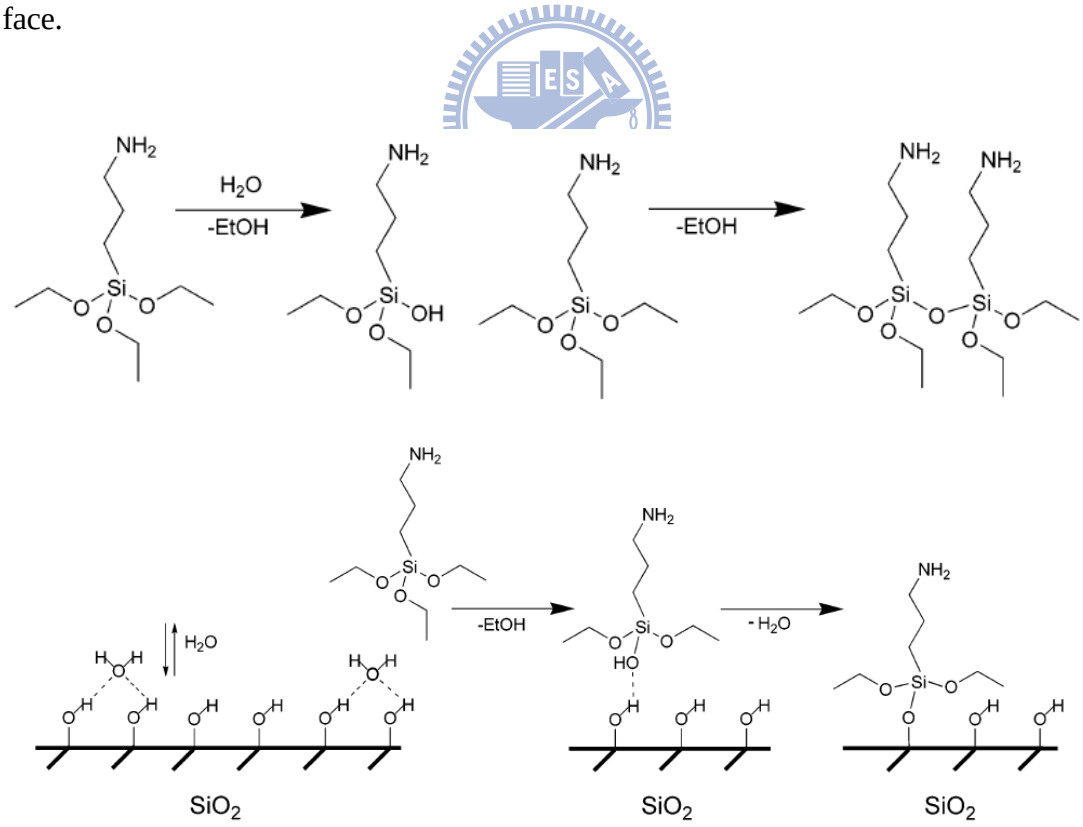

Fig. 2-4 Chemical mechanism of APTES coating. APTES hydrolysis is followed by condensation reaction in solution phase. Bottom scheme of APTES hydrolysis is followed by condensation at hydrated silica surface.

2.2 Literature about BioFET application

The detection of biological and chemical species is central to many areas of healthcare and the life sciences, ranging from uncovering and diagnosing disease to the discovery and screening of new drug molecules. Hence, the development of new devices that enable direct, sensitive, and rapid analysis of these species could impact humankind in significant ways. Devices based on nanobelts are emerging as a powerful and general class of ultrasensitive, electrical sensors for the direct detection of biological and chemical species. [45]. Bashir and co-workers [28] described SiNW-FET sensor process that was realized using the top–down microelectronics processing techniques. A process known as confined was utilized to obtain single crystal silicon nano-plates that are thin as 7nm and nanobelts small as 40nm in diameter at precise locations, as shown in figure 2-5 [29]. The method allows the realization of truly integrated dense array of sensor. Initial testing of the device showed that sensitivity towards oxygen ambient, and suggested it possibility of using these sensors for chemical and biological detection shown (figure 2-6) [28].

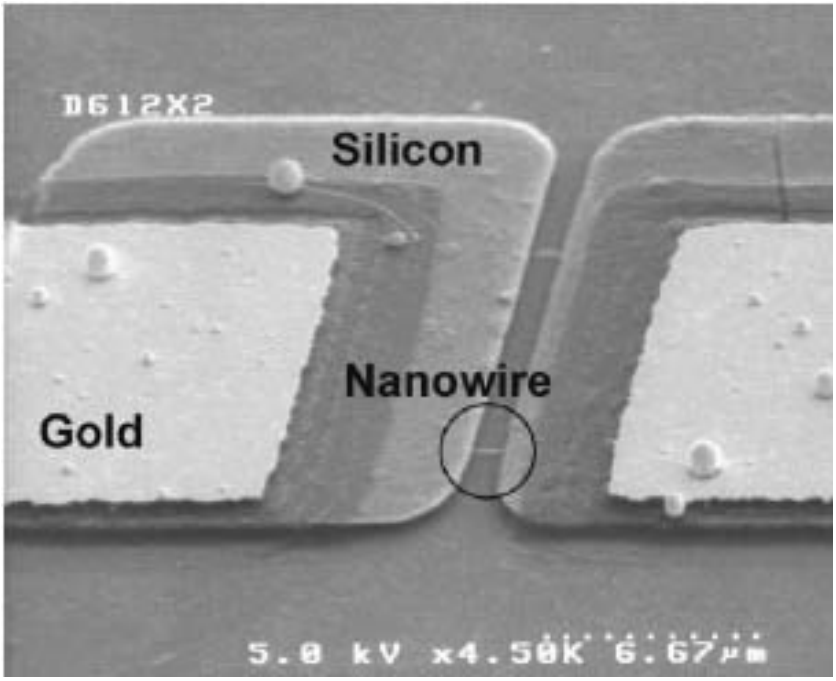

Fig. 2-5 Field emission scanning electron microscopy photos of the fabricated devices. There are two nanowire between electrodes.

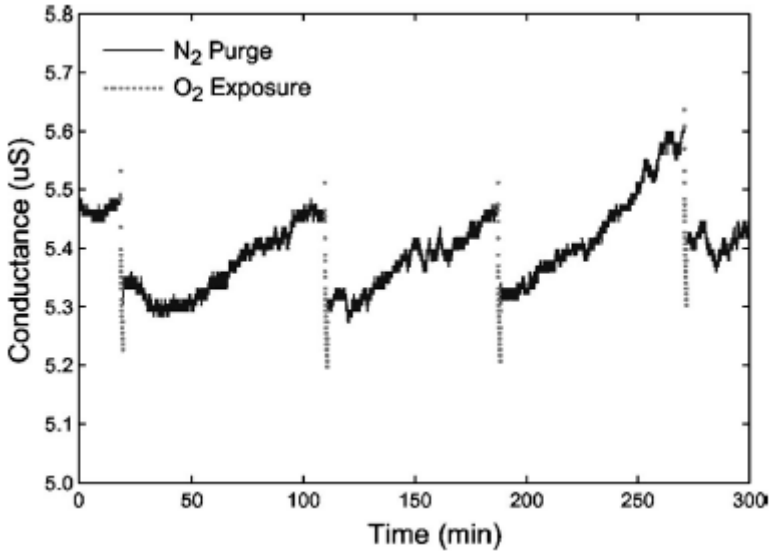

Fig. 2-6 Gases responded by nanowire devices. Electrical current of the device is responded to oxygen and nitrogen. Initial testing of the device showed that sensitivity towards oxygen ambient.

Li et al.[30, 31] fabricating a single crystal silicon nanobelt is with 50 nm and in width on SOI wafer by electron beam lithography. They have demonstrated the detection of DNA molecules based on their intrinsic charge by using SiNWs fabricated by top-down semiconductor processes. This method created a pathway for high-density, high-quality, and well organized nanoscale sensor that can be integrated with communication circuits, as shown in figure 2-7 [30]. Sequence-specific and label-free DNA sensors based on SiNW with probe-DNA or PNA molecules covalently immobilized on the surfaces (figure 2-8) [31]. Complementary DNA was recognized when the target DNA was complementary with the probe-DNA attached onto the SiNW surfaces, causes the change to accumulate on the surface of the SiNW.

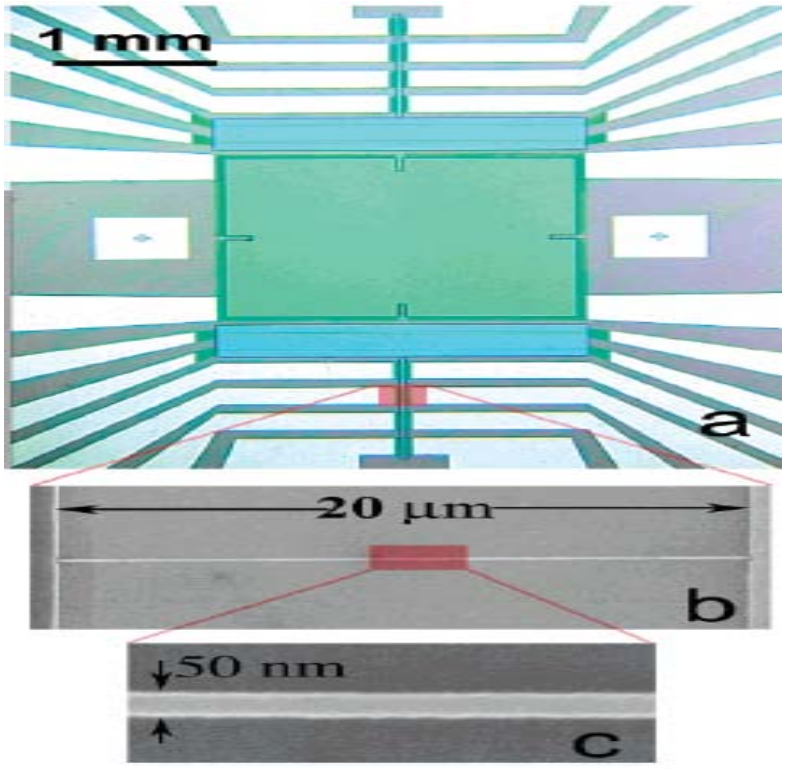

Fig. 2-7 Optical and SEM image of nanowire sensor. (a) The optical image of the central region of a sensor used for the DNA sensing study. (b) and (c) Representative SEM images showing the SiNW bridging two contact leads.

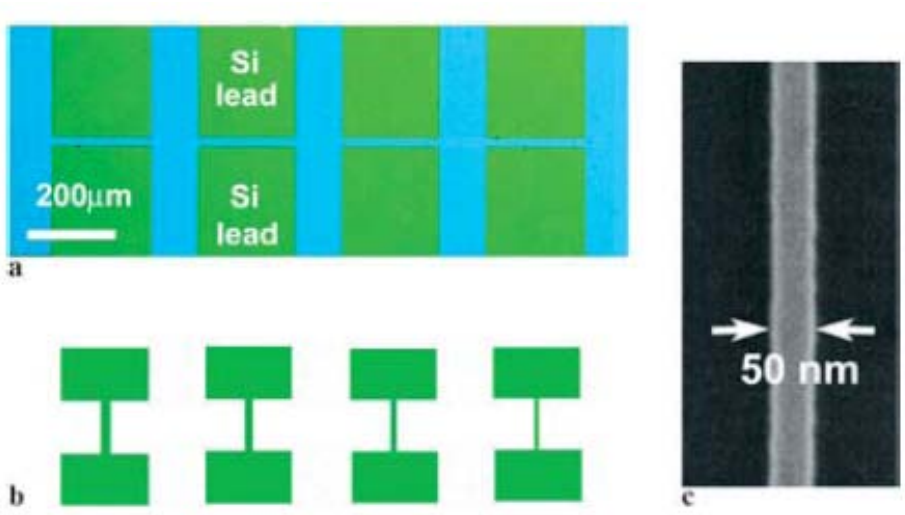

Fig. 2-8 Optical and SEM image of nanowire sensor. (a) Optical image of the central region of a sensor showing a portion of the lead and the bridged nanowire used for the DNA sensing; (b) schematic drawing of the SiNW with varying widths corresponding to the image in (a); (c) a SEM image showing a 50-nm-wide SiNW, which extends between two contact leads.

Sheu et al. [32] demonstrated the bio-detection by using the SiNW whose surface was pretreated by APTMS and then selectively deposited with gold nanoparticles, as shown in figure 2-9 and figure 2-10 [32]. The GNPs on the surface served as linkers for detection. The target molecules bound with GNPs on the surface of the SiNB and resulted in a voltage shift.

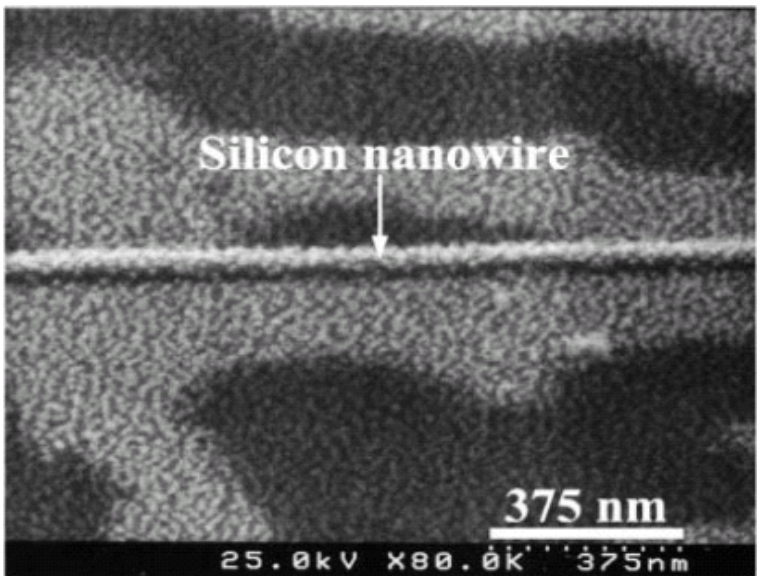

Fig. 2-9 SEM image of SiNW after reaction of the GNPs with APTMS.

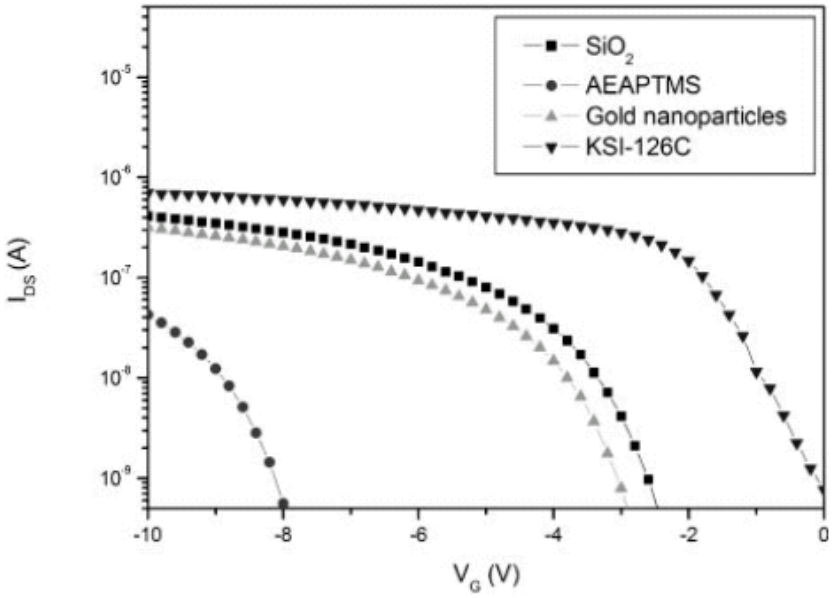

Fig. 2-10 I_D-V_G curves of SiNW after binding of different molecules on the surface of SiNW. The turn-on voltage was changed after binding of different molecules

Ko et al. [33] developed a self-aligned platinum-silicide nanobelt (figure 2-11) for biomolecules sensing. The immobilization steps of the DNA onto the nanobelt are illustrated in figure 2-12. The 40 nm-width nanobelt is fabricated through a sequence of electron-beam writing on the poly-Si film, line shrinking by alkaline solution, pla-

tinum film depositing, 550 ℃ annealing, and aqua dissolution is performed. The immobilization of capture-DNA on the platinum-silicide nanobelt is verified from the fluorescence-labeled technique. The FET can distinguish the complementary, mismatched, and dehybridized DNA via the conductance difference. They can sense the minimal target DNA concentration down to 100 fM.

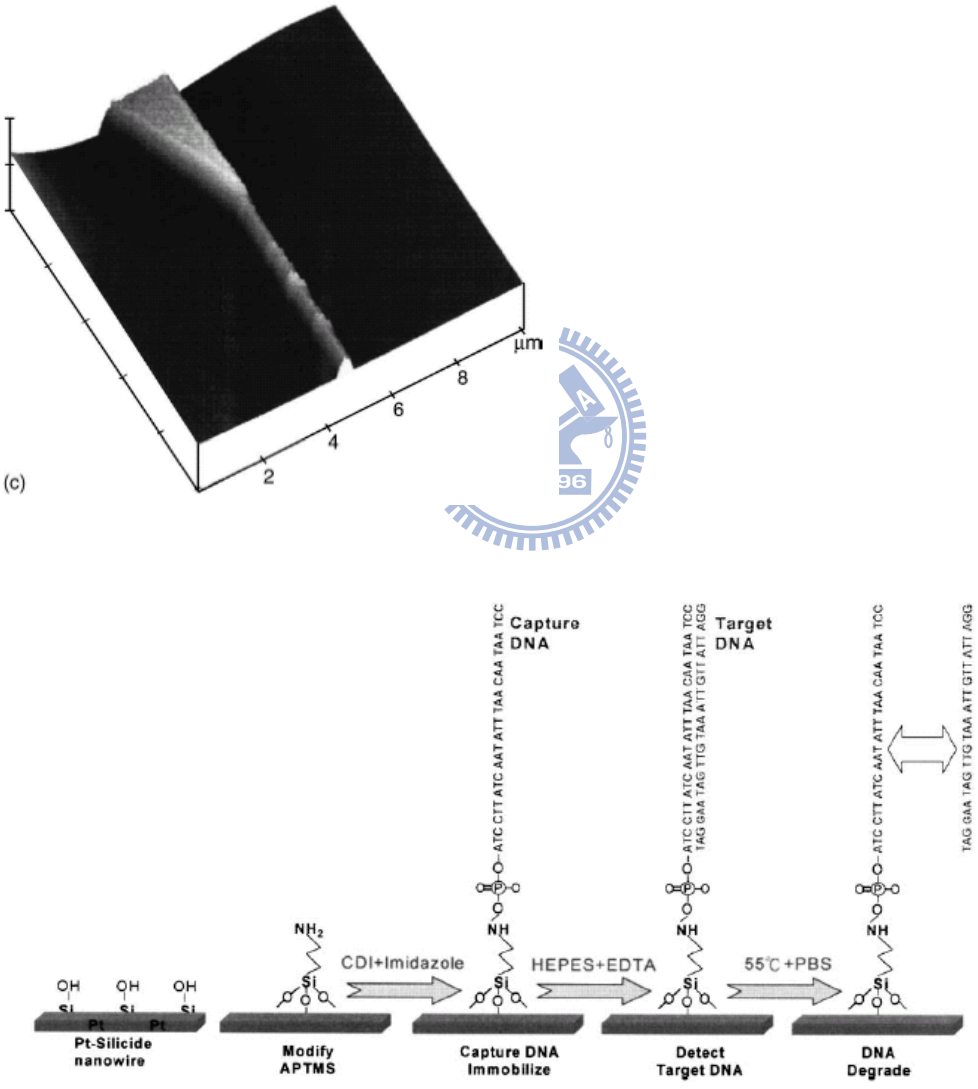

Fig. 2-11 The 3-D AFM image of 40 nm width Pt-silicide nanowire, and the immobilization steps for the DNA on the Pt-silicide nanowire.

Eric Stern et al. [34] have demonstrated an approach to realize the characteristic of the SiNW sensors for specific antibody detection. The images and electrical properties of the SiNW sensors are shown in figure 2-13. This approach has the potential for extending single device to an integrated system, with widely use as the chip-arrays. Successful solution-phase nanowire sensing has been demonstrated for ions [30, 31], proteins [32, 33], and DNA [34]. However, top-down fabrication of nanobelt devices [35, 36, 37] produced. Here they reported the uses of CMOS-FET compatible technology and hence demonstrate the specific label-free detection of antibodies as well as real-time monitoring of the immune response.

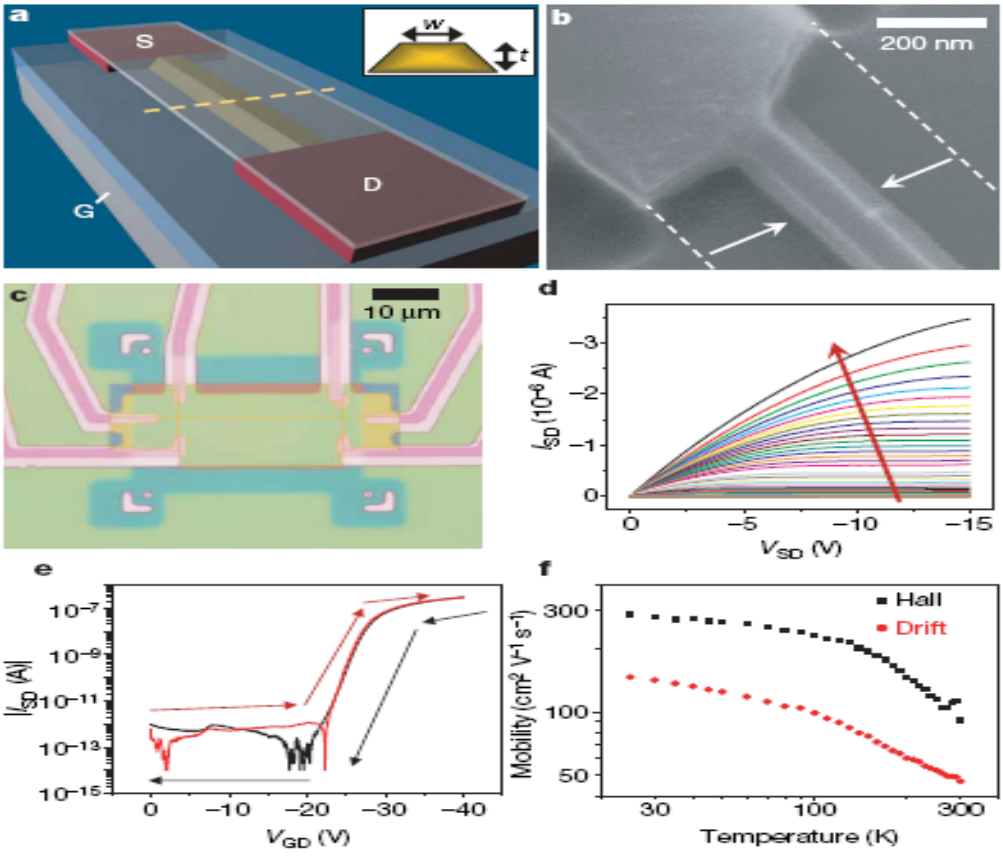

Fig.2-12 Device fabrication and electrical performance. (a) Schematic of active channel. The source, drain, and back-gate are labeled; (b) SEM and (c) OM image of a device; (d) ISD for varying VGD, illustrating p-type behaviour; (e) ISD for VGD

for forward and reverse sweep. (f) Hall and drift mobilities versus temperature.

Pritiraj Mohanty et al. [38] demonstrated the fabrication, functionalization, and operation of a nano-electronic FET for pH sensor, as shown in figure2-14. The SiNW with back-gate is fabricated with standard semiconductor process. The functionalized SiNW can be controlled with local back-gate to induce inversion or depletion layers. This approach offers the possibility of highly parallel detection of ion or charged protein and DNA with control of individual elements. By selective gating, individual NWs in an array can be turned on or off during sensing process. Therefore, the array contains multiple receptors for the detection of multiple chemical and biological species in a single integrated chip.

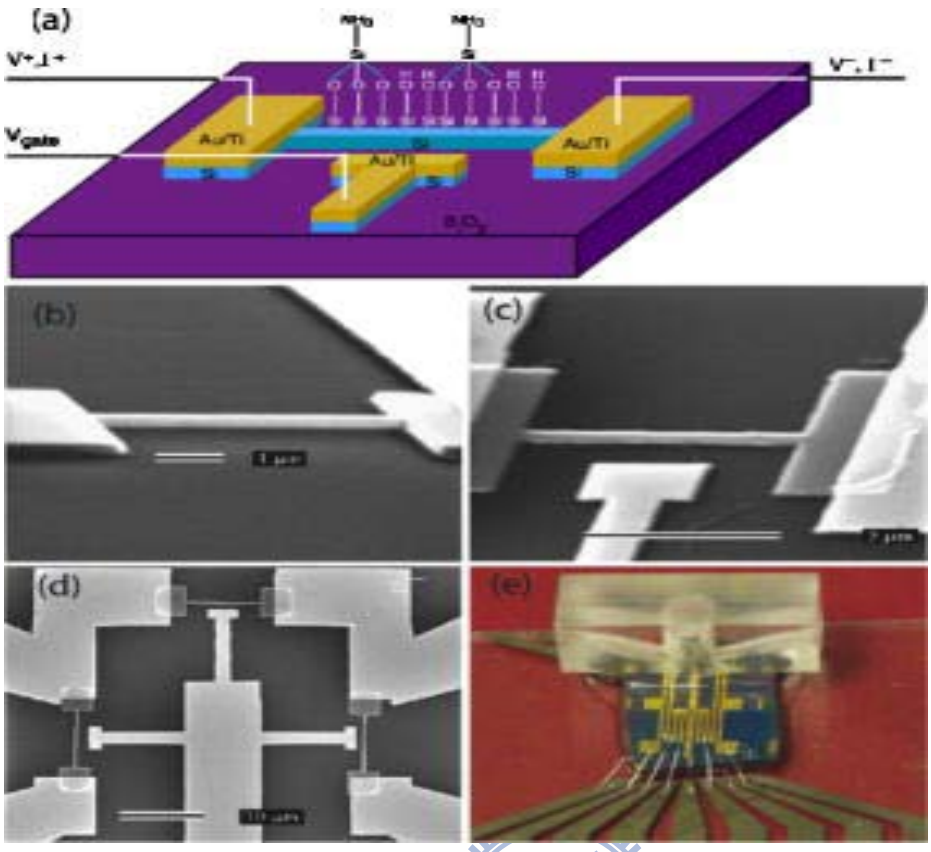

Fig. 2-13 Device schematic diagram. (a) The diagram of the SiNW with back-gate; (b) The nanowire shown here; (c) A SiNW with a Au/Ti back-gate. (d) The SEM image displays three SiNW devices on the same chip; (e) An OM image shows the flow chamber sealed on top of the devices.

2.3 Real-time Nanobelt Field-Effect-Transisitor Biosensors

Detectors based on semiconductor NWs are configured as FETs, which exhibit a conductivity change in response to variations in the electric field or potential at the surface [35]. The dependence of the conductance on gate voltage makes FETs natural candidates for electrically based sensing, because the electric field resulting from the binding of a charged species is the effect of applying a voltage with a gate electrode. They can be prepared as p- or n-type materials and configured as FETs in Figure

2-15(b) that exhibit electrical performance characteristics better achieved for planar silicon devices [39, 40, 41]. The superior switching characteristics of SiNWs are among the most important factors that affect sensitivity. The binding of biomolecules onto the surface of the NW leads to depletion or accumulation of carriers, versus only the surface region of a device. This semiconductor NWs provides sufficient sensitivity to enable the detection of importing biomolecules in solution. However, because these are field-effect devices, detection sensitivity depends on the ionic strength of the solution. A sensing device can be configured from high-performance NW FETs by linking NW receptor groups that recognize specific molecules to the surface of the NW in figure 2-15(c). When the sensor device with surface receptors is exposed to a solution containing biomolecules, such as protein that has net negative charges in the aqueous solution, specific binding will lead to an increase in the surface and in conductance for a p-type NW device. As a proof of concept, they have developed a microfluidic system integrated NW sensor that incorporates SiNWs with well-defined p- or n-type doping; source and drain electrodes that are insulated from the aqueous reagent environment, so that only processes occurring at the SiNW surface contribute to electrical signals; and a microfluidic channel for delivery of solutions in Figure 2-15(d) [42]. They fabricated electrically addressable arrays by a process that uses fluid-based assembly of NWs to align them and spacing over large areas [42]. Photolithography and metal deposition define interconnections to a large number of individual NWs in parallel in Figure 2-16.

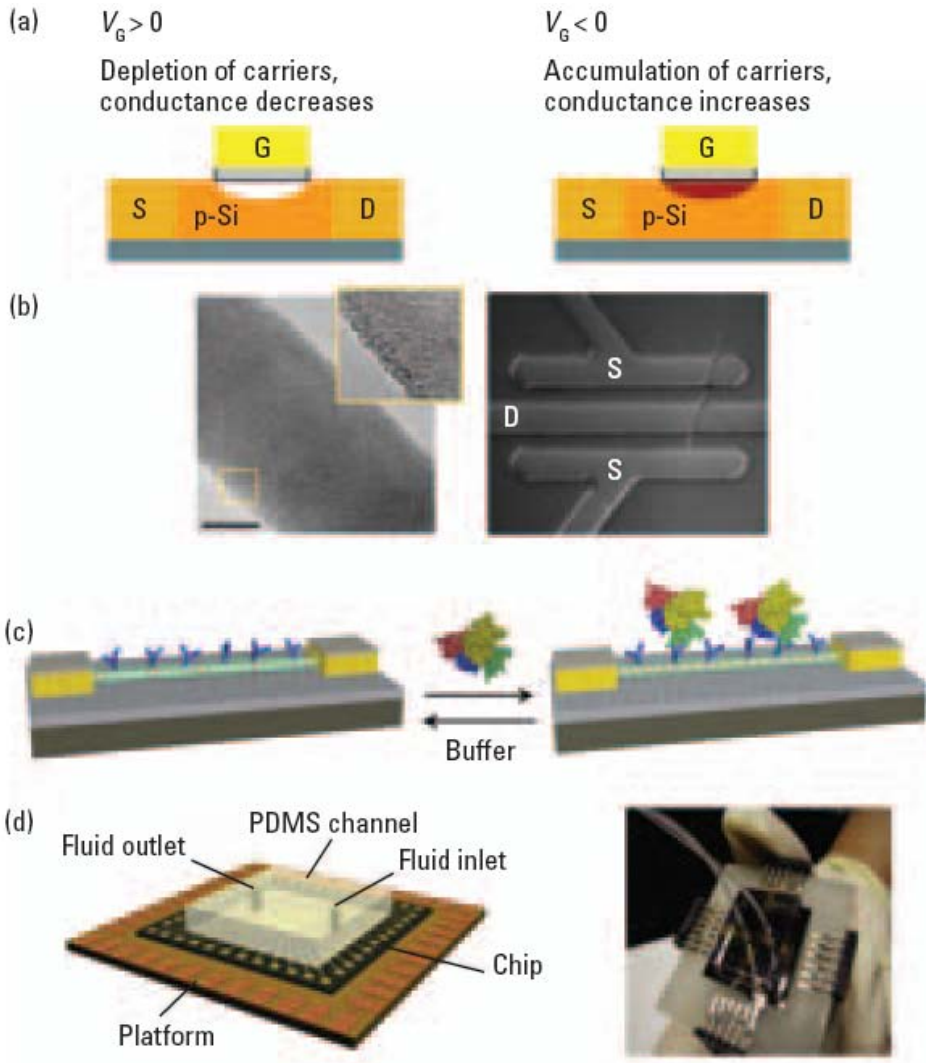

Figure 2-14 NW-FET sensors. (a) Schematic of a p-type FET device. S, source; D, drain; and G, gate electrodes; VG, gate voltage; (b) (left) TEM images of a 20-nm-diam single-crystal SiNW and (right) an OM image of a device; (c) Schematic of a sensor with antibody receptors (blue); binding of a protein with a net negative charge results in an increase in conductance; (d) NW sensor biochip with integrated microfluidic sample delivery.

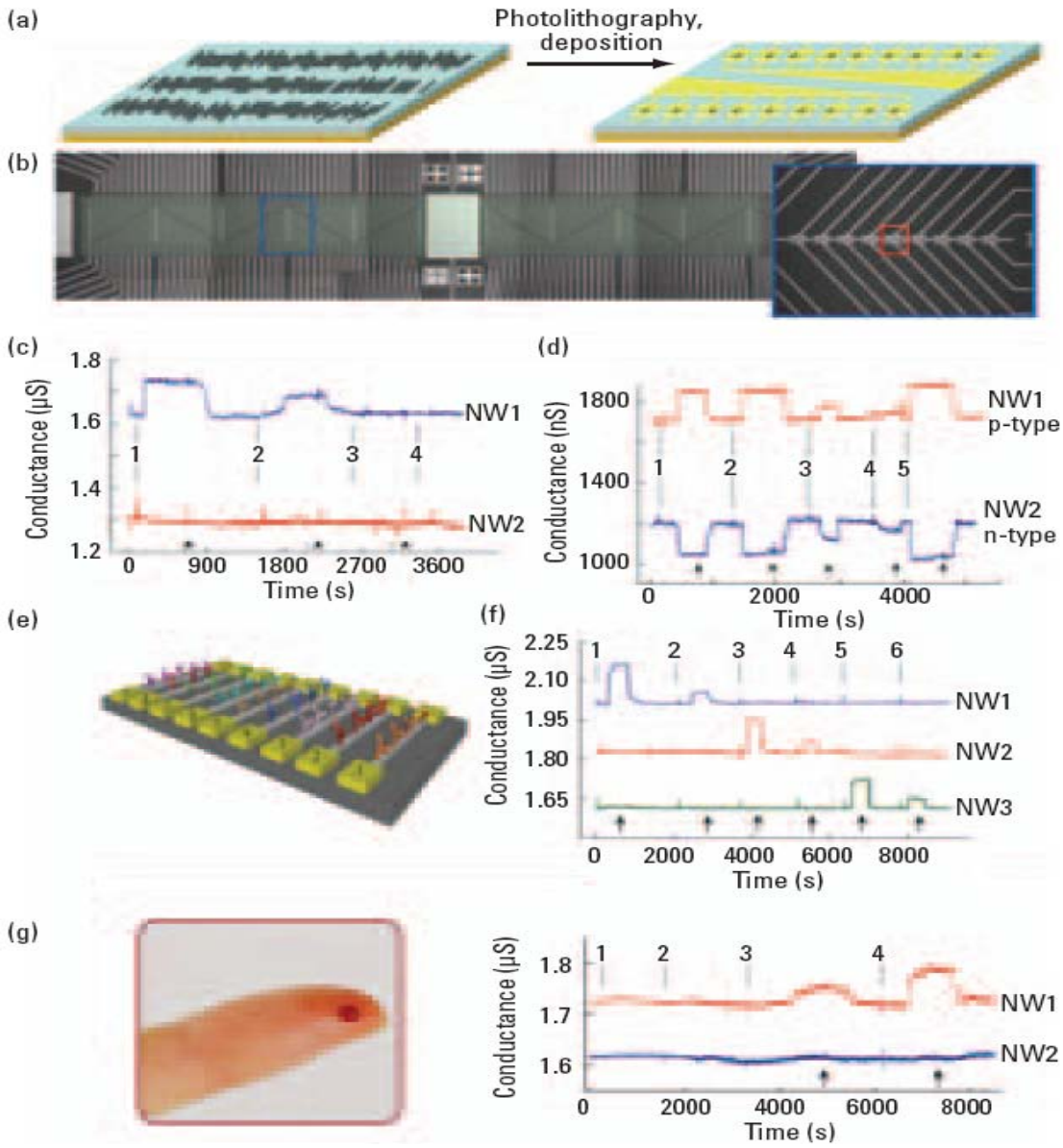

Fig. 2-15 NW arrays for multiplexed protein sensing. (a) Illustration of NW array fabrication; (b) Optical image of a NW array; (c) Data recorded from p-SiNW devices; NW1 was immobilized with PSA-Ab1, and NW2 was modified with ethanolamine; (d) Complementary sensing of PSA with p-type (NW1) and n-type (NW2) NW devices; (e) Schematic of array detection of multiple proteins; (f) Detection of PSA, CEA, and mucin-1 with NW1, NW2, and NW3 functionalized with antibodies. Protein solutions of PSA, CEA, and mucin-1 were delivered sequentially to the array. (g) The drop of blood corresponds to the quantity required for analysis. Conductance versus time data recorded for the detection of PSA and PSA. NW2 was passivated

with ethanolamine.

Recently, the biosensor has employed increasingly in a variety of applications where continuous measurements in biological media are required by real-time monitoring sensing. An electrochemical biosensor has been defined as a “self-contained integrated device, which is capable for providing specific quantitative or semi-quantitative information using a biological recognition element retained in direct spatial contact with an electrochemical transduction element” [42]. A biosensor is distinguished from a chemical sensor in that it possesses a biological recognition element, typically a protein, peptide or oligonucleotide. The goal in this subject may measure the rate of uptake or efflux of relevant species or to establish spatial distributions in real-time sensing. [43]. When a sensor is brought in contact with biological tissues, sensor performance can deteriorate. The exact causes of this deterioration are not clear, but are a mix of passive adsorption of biomolecules on the sensor probe surface and active processes coupled to tissue response [43]. For this reason, we will give some attention to approve the microfluidic system that can play key roles in regulation of detection events. This affords a greater range of analytical approaches to analysis, including separations and derivatization not possible with a single real-time sensor array.

Chapter 3: Experimental and material

3.0 Experimental process

The whole experimental procedure will divide into ten parts: (1) Fabrication of back-gated Silicon Nanobelt Field-Effect Transistor (NWFET), (2) self-assembly of APTES on the NWFET device for detection pH value of solution, (3) self-assembly of capture DNA on the NWFET device, (4) self-assembly of Antibody on the NWFET device, (5) fluorescence labeled capture DNA, (6) PDMS sample channel fabrication, (7) assemble the FET sensor to the whole system, (8) prepare the pH degree solution, (9) prepare the HBV gene, (10) Prepare the AFP sample in vitro or in vivo. These ten parts are not continuous process, and they will be discussed in more details in the following section.

3.1 Fabrication of back-gated silicon nanobelt field-effect transistor (NB FET)

A back-gated nanobelt's FET sensor was fabricated by using commercially available 6-in. (100) silicon-on-insulator (SOI) wafers as the device substrate. The stacked films of TEOS-oxide and silicon nitride were deposited sequentially as the masking layer for local-oxidation of silicon (LOCOS) process. The underlying layer of TEOS-oxide, called a pad oxide, is used to cushion the transition of stresses between the silicon and the nitride film. The active region and gate were then defined by the optical lithography system (Canon FPA-3000i5 stepper). The composed oxide/nitride stack layers were then plasma-etched, followed by the oxidation process was thermally grown. The patterned silicon nitride prevented the underlying silicon from oxidation and left the exposed silicon to be oxidized. As a result, the

active region including nanobelt, source, drain, and gate were defined due to the silicon nitride capped on top of the regions. In addition, the linewidth of nanobelts were shrunk due to oxidant diffused laterally during the oxidation process. This phenomenon, the “bird’s beak” effect, could induce the linewidth of nanobelts smaller than the critical width of the exposure system’s capability.

After the active region was patterned, As^{+} ion implant and rapid thermal anneal were carried out to form the source, drain, and gate region. Prior to defining the contact pad region by lithography and etching, the stacked Al-Si-Cu alloy onto titanium nitride metal film was formed by sputter system. Then, the silicon dioxide and silicon nitride layers were deposited to passivate the surface. The whole procedure was completed in National Chiao Tung University (NCTU) [1] or National Nano Device Laboratories (NDL) [2]. All of the medicine, reagents, and solvents were reagent-grade quality or higher level. The detection region of the back-gated NBFET was then etched back for the purpose of DNA immobilization. A schematic diagram of the fabricated back-gated NBFET biosensor is depicted in Fig. 3-1. The device after fabrication was stored in the clean room.

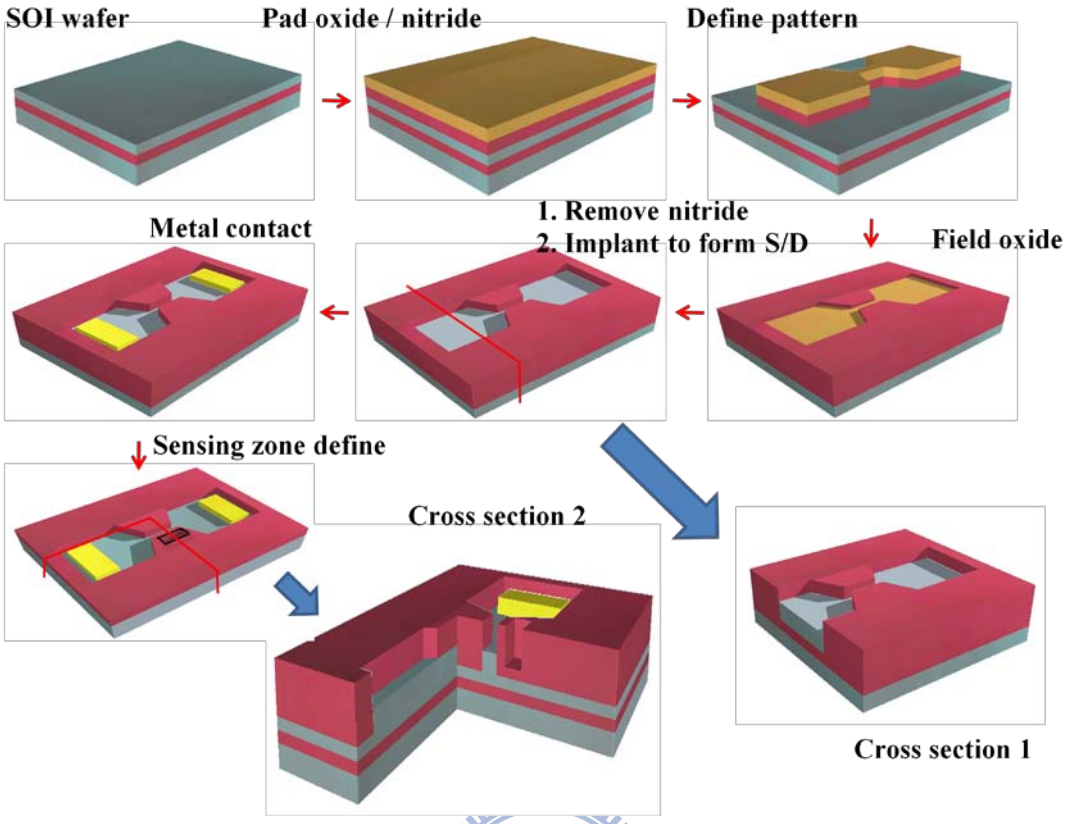

Fig. 3-1 Schematic Diagram of the NB FET fabrication process. Back-gated nanobelt's FET sensor was fabricated by using 6-in. (100) silicon-on-insulator (SOI) wafers as substrate. The stacked films of TEOS-oxide and silicon nitride were deposited sequentially. Following coated the pad oxide. The active region and gate were then defined with the electron-beam writer. The composed oxide/nitride stack layers were then plasma-etched, followed by the oxidation process was thermally grown. After the active region was patterned, As^{+} ions implant and rapid thermal anneal were carried out to form the source, drain, and gate region. The sensing zone of the back-gated NBFET was then etched back for the purpose of DNA immobilization.

3.2 Self-assembly of APTES on the NBFET device for solution pH detection

Prior to immobilizing APTES, sensors were cleaned for 30 min using acetone and ethanol mixture for 1:1. High purity DI water, purified through double deionization processes, was used throughout. After cleaning process, a monolayer of APTES was then immobilized onto the NBFET surface (figure 3-2). The surface reactions occurred with the silanol groups present on the silicon NB surface as a result of native oxide formation. Because silanol groups and APTES are good proton (H^+) donors and acceptors, solution pH was hence detected by the variation of ions.

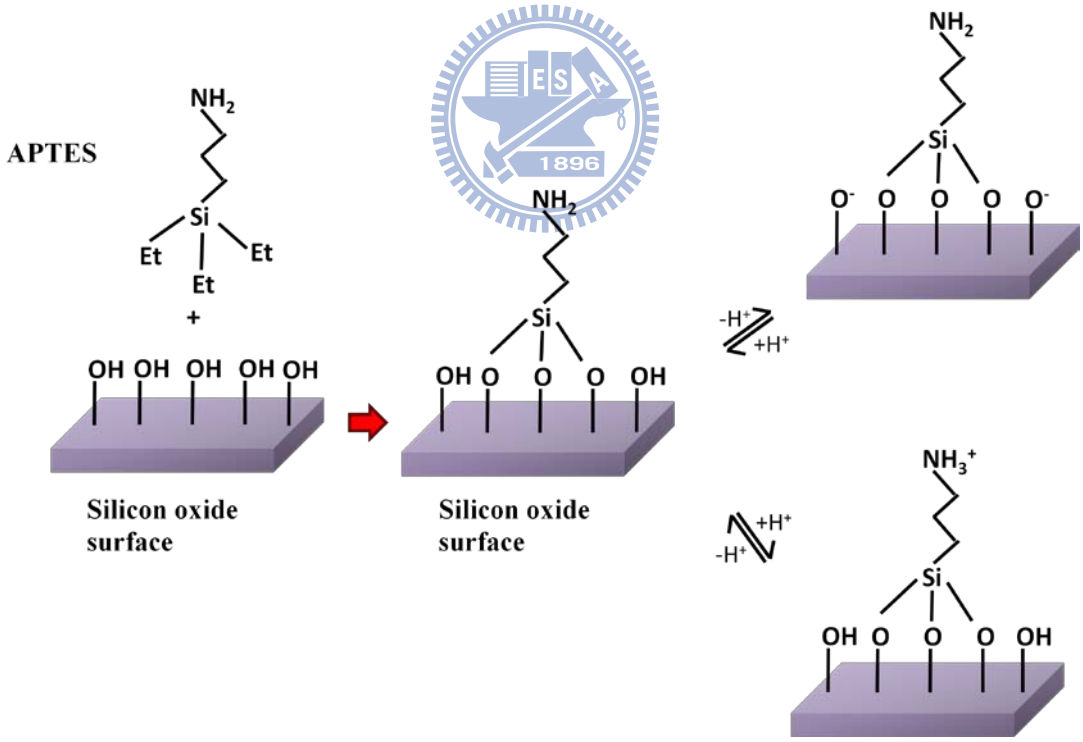

Fig. 3-2 Procedure of APTES immobilization on the NBFET surface. APTES reactions with the silanol groups present on the silicon NW surface. Silanol groups and APTES on SiNB are applied for pH sensing.

3.3 Self-assembly of capture DNA on the NBFET device

After cleaning process described in section 3.2, a monolayer of 20-mer single-stranded DNA (named capture DNA, Blossom Biotechnologies, Taipei, Taiwan) molecules was then immobilized onto the NBFET surface. The surface reactions occurred with the silanol groups present on the silicon NB surface as a result of native oxide formation. APTES and glutaraldehyde was employed as linker to self-assemble a monolayer of DNA onto the surface of NB detection region. Figure 3-3 illustrates the procedure for immobilization of the DNA molecules onto the surface-bounded APTES molecules. Initially, the samples were immersed into a 10% APTES aqueous solution for 30 min at 37 °C and adjusted to pH 3.5 with 1 M hydrochloric acid. The samples were then rinsed with DI water and dried on a hot plate (120 °C for 30 min). At this stage, amino groups were presented as terminal units on the surface. Next, glutaraldehyde was linked to the amino groups to present aldehyde groups on the surface; the sample was immersed in the linker solution [2.5% glutaraldehyde (1,5-pentanedial)] for 30 min at room temperature and then rinsed with phosphate-buffered saline (PBS, 120 mM NaCl, 2.7 mM KCl, and 10 mM phosphate buffer; pH 7.4; Sigma–Aldrich) solution (Yoshida et al., 1995). The 2.5% glutaraldehyde solution (Stefano et al., 2008; Yakovleva et al., 2002) was diluted with PBS solution from 25% glutaraldehyde (Sigma–Aldrich). Next, the selective immobilization technique was used to bind the terminal 3´-amino group of the oligonucleotide to the aldehyde groups on the NW surface. A fresh solution of synthetic 1 μM capture DNA (Blossom Biotechnologies, Taipei, Taiwan) was diluted with PBS buffer to provide a 10 nM solution of capture DNA. A portion (100 μL) of this capture DNA solution was dropped onto the NBs and reacted for 1 h to ensure effective immobilization. The un-reacted aldehyde groups were blocked by ethanolamine

(Sigma–Aldrich), washed with PBS buffer, and subsequently dried under ambient nitrogen.

To ensure the immobilization efficiency of capture DNA, a fluorescence-labeled capture DNA (Blossom Biotechnologies, Taipei, Taiwan) was also prepared. The fluorescence used here was fluorescein isothiocyanate (FITC), which was specifically modified in the 5' end of the capture DNA. Green fluorescence images (excitation: 494 nm; emission: 520 nm) were observed using a BX51 fluorescence microscope (Olympus, PA, USA).

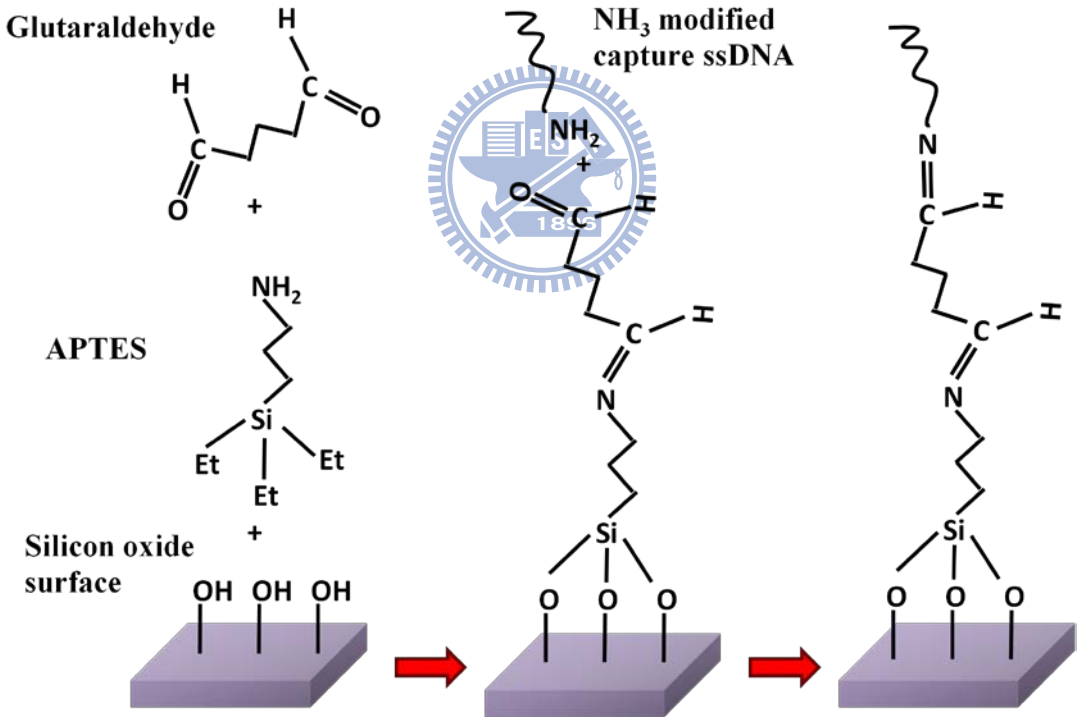

Fig. 3-3 Procedure of DNA Immobilization on the NBFET surface. APTES and glutaraldehyde were employed as linker. In the next immobilization the terminal 3´-amino group modified DNA, this functional DNA is used as a capture molecular in order to binding the HBV X gene DNA fragment.

3.4 Self-assembly of antibody on the NBFET device

The AFP antibody was first diluted to 10 nM, and (Fitzgerald Industries International, Inc. USA) was then modified on the NBFET surface. The surface reactions occurred with the silanol groups present on the silicon NB surface as a result of native oxide formation. Figure 3-4 illustrates the procedure for immobilization of the protein molecules onto the surface-bounded APTES molecules. Initially, the samples were immersed into a 10% APTES anhydro solution for 30 min at 37 ℃. The samples were then rinsed with DI water and dried on a hot plate (120 ℃ for 30 min). At this stage, amino groups were presented as terminal units on the surface. Next, glutaraldehyde was linked to the amino groups to present aldehyde groups on the surface; the sample was immersed in the linker solution [2.5% glutaraldehyde (1,5-pentanedial)] for 30 min at room temperature and then rinsed with phosphate-buffered saline (PBS, 120 mM NaCl, 2.7 mM KCl, and 10 mM phosphate buffer; pH 7.4; Sigma–Aldrich) solution. The 2.5% glutaraldehyde solution was diluted with PBS solution from 25% glutaraldehyde (Sigma–Aldrich). Next, the selective immobilization technique was used to bind the amino group of the antibody onto the aldehyde groups on the NB surface. The un-reacted aldehyde groups were blocked by ethanolamine (Sigma–Aldrich), washed with PBS buffer, and subsequently dried under ambient nitrogen.

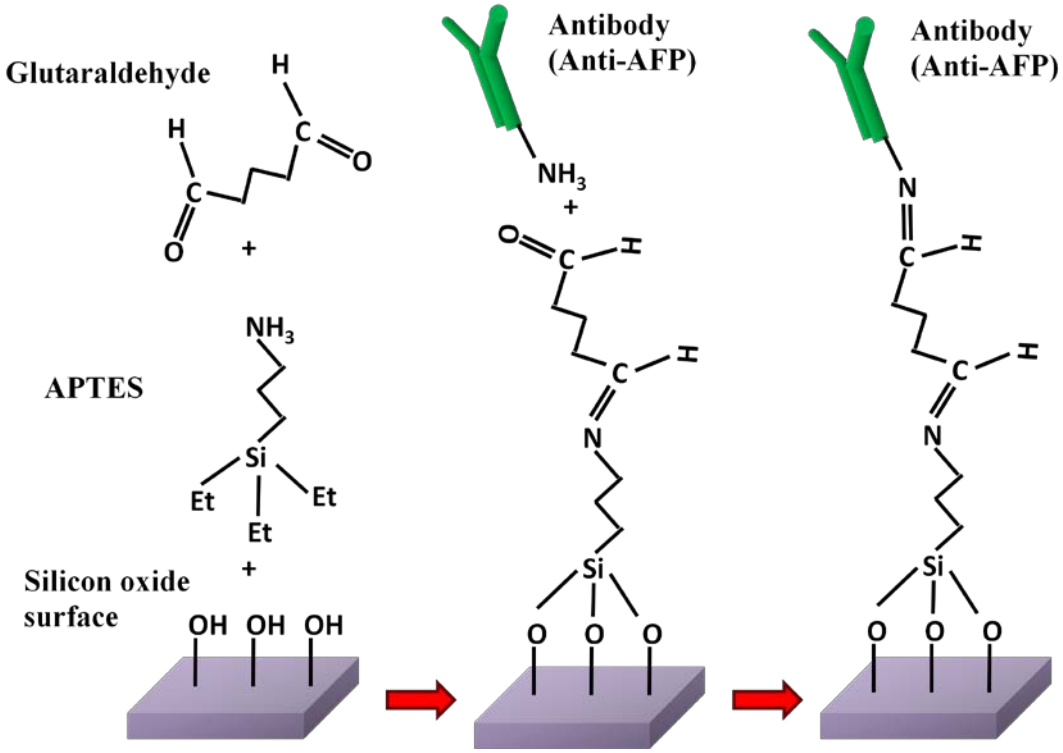

Fig. 3-4 Procedure of antibody coated on SiNB. APTES and glutaraldehyde was employed as linker for coated anti-AFP anti body for AFP sensing. The anti-AFP we used has a amino group in its constant region for reduce with aldehyde group of glutaraaldehyde.

3.5 Fluorescence labeled capture DNA

To ensure the immobilization efficiency of capture DNA, a fluorescence-labeled capture DNA (Blossom Biotechnologies, Taipei, Taiwan) was also prepared. The fluorescence used here was fluorescein isothiocyanate (FITC), which was specifically modified in the 5' end of the capture DNA. A fluorescence images (excitation: 494 nm; emission: 520 nm) were observed using a BX51 fluorescence microscope (Olympus, PA, USA), in order to ensure that the capture DNA exactly coated on the sensing zone of our BioFET type sensor.

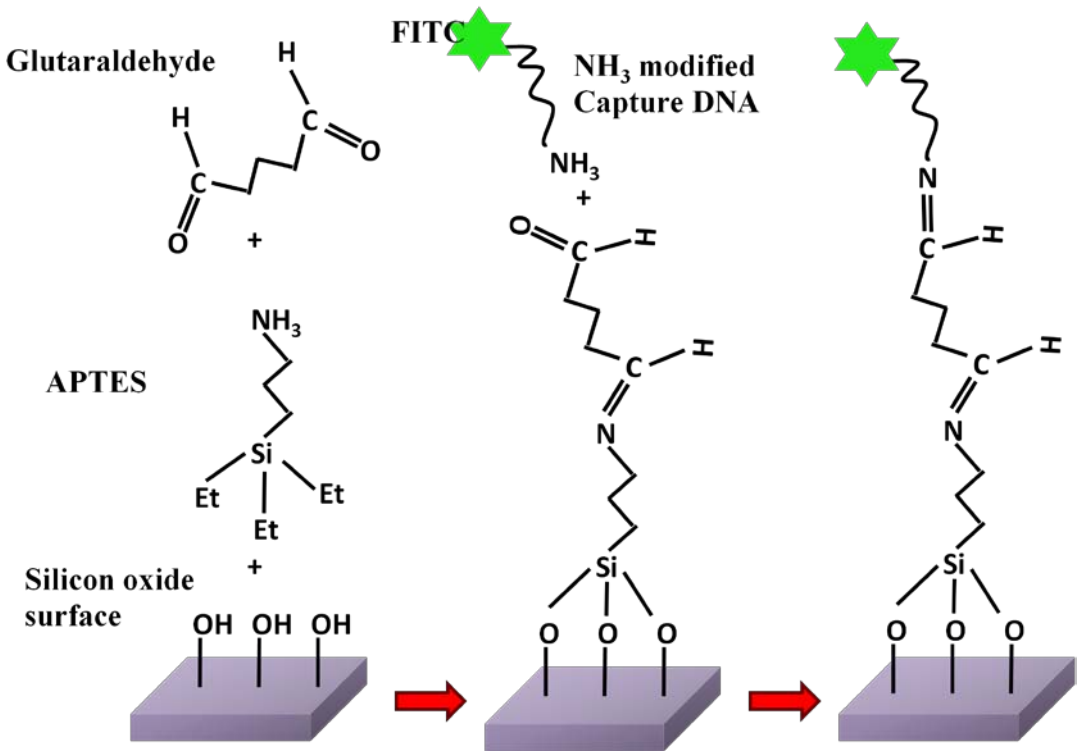

Fig. 3-5 Procedure of FITC-DNA immobilized. APTES and glutaraldehyde was employed as linker for FITC-DNA immobilized. A fluorescence images (excitation: 494 nm; emission: 520 nm) were observed using a BX51 fluorescence microscope.

3.6 PDMS sample channel fabrication

The fabrication of the microfluidic channel and integration with the NWFET is a necessary step for automatic sample delivery. We manufacture PDMS (sylgard 184A) to form structure, which contain a sample delivery channel. The PDMS is purchase from Sil-More Industrial Ltd.

The PDMS was mixed with the cure agent for 10:1, the mixture was then dropped to the 10 cm dish container. The 10 cm dish container was prior fixed with the 50 um in-diameter iron rod as the mold of channel. After pumping out the micro bubble and the froth inner PDMS, the PDMS was dried bake at 70℃ in an oven for four

hours. The next is the drawing of pattern, and cutting the PDMS to I-shape structure. The following figure is the process of I-shape channel and the cross section of the channel.

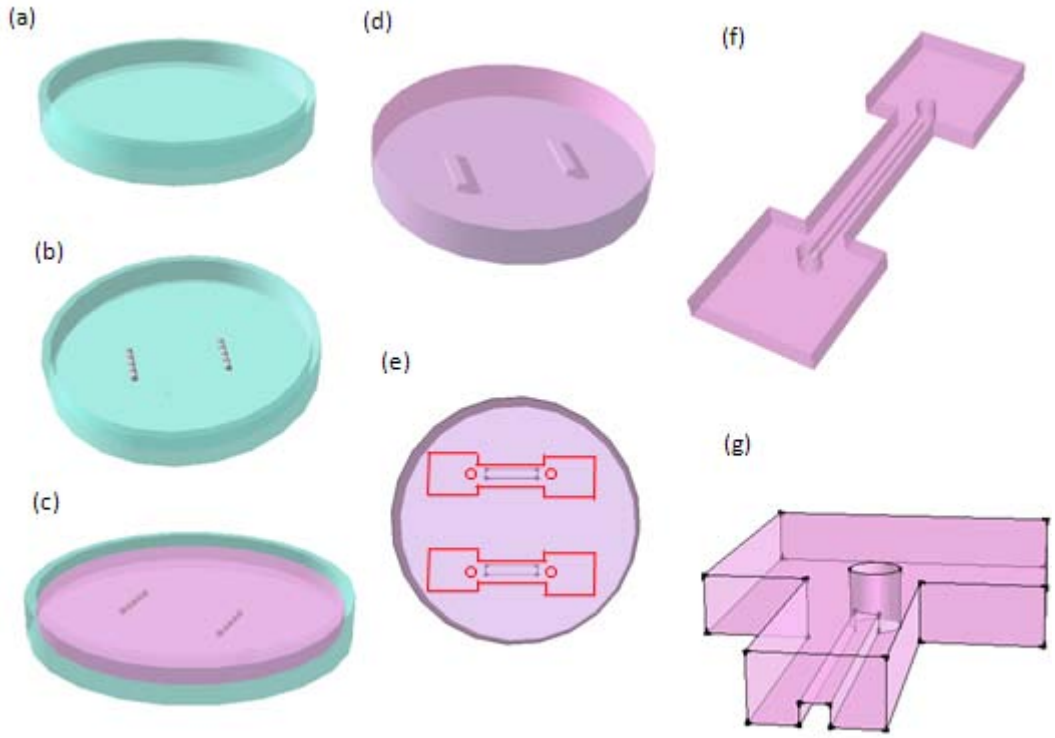

Fig 3-6 Schematic diagram of the microfludic channel fabrication process. (a) 10 cm dish. (b) Metal rods are immobilized on the 10 cm dish to create the chaneel mold. (c) Mixed the PDMS with the cure agent (10:1), and dropped the mixture to the 10 cm dish container. (d)Pumping out the micro bubble and the froth inner PDMS, the PDMS will dry bake in 70℃ for four hours. (e) Drawing of pattern of the microchannel.(f)Cutting the PDMS microchannel to I form structure. (g) Cross section of the channel.

3.7 Assemble the FET sensor to the system

We used the metal holder and acrylics gasket to clip the FET sensor and I-shape PDMS channel to prevent samples leakage. We used plastics tube for sample transfer and waste liquid exported. Finally, the syringe pump was employed as a motive

power to automatic sample transmission.

3.8 Preparation of the pH degree solution

In general, a health people has body fluid or blood that pH value is between 7.35-7.45, sometimes also called alkaline body chemistry. Therefore, the pH range for cells to survive in the internal environment is quite narrow. In general, PH under 7.35 may be considered acidosis, and PH over 7.45 may be considered alkalosis. Some more deviation, with PH under 7.30 or PH over 7.50, means more severe acid-base imbalance, which can be life-threatening. When a human is infected to cancer, the blood pH usually decreased, this is a good reason for us to utilize pH detection of blood to know the health situation of our body.

We dissolved the phosphate buffered saline pill (P4417-100TAB, purchase from SIGMA) into 200 ml DI water. The NaOH and HCl was used to modulate the pH of sample. We prepared pH value of 6.4-7.4 to test the FET sensor pH detection ability. The pH sample was simulated the healthy, sub-healthy, and disorder physiological fluid of our body.

3.9 Preparation of the HBV X gene DNA fragments

Recent study indicated that the HBV DNA will leakage to the plasma through its replication circle. All HBV x gene fragments we use as sample is synthesis by chemistry procedure (purchase from MDBio[3-5], Inc.), the DNA sequence we applied is list in following table. All the DNA are dissolve in PBS buffer (pH 7.4), and stored in -20℃.

Sequence of the capture DNA	5'-NH2-ACGTCCCGCGCAGGA-3'
Sequence of target DNA	5'-TCCTGCGCGGGACGT-3'
Target DNA with 1 base mismatch	5'-TCCTGCGAGGGACGT-3'
Target DNA with 5 bases mismatch	5'-TCCTGACACTGACGT-3'
Non-complimentary DNA	5'-GAACCACACTAGATG-3'

Table 3-1 Lists of the capture, target, one-base, five-base, and non-complementary DNA sequence. *Sequence of the capture DNA* is the fragment of DNA that complementary to the HBV X gene, which we coated on the SiNB FET sensor; *Sequence of target DNA* is DNA fragment whice sequence is mimic the HBV X gen DNA sequence; *Target DNA with 1 base mismatch* is complementary to the *Sequence of the capture DNA* but with one base mismatch in the medium; *Target DNA with 5 bases mismatch* is complementary to the *Sequence of the capture DNA* but with five base mismatch in the medium; *Non-complimentary DNA* is a random sequence which cannot hybrid to *Sequence of the capture DNA.*

3.10 Preparation of the AFP sample in vitro or in vivo

AFP (AFP, α-fetoprotein) is a protein [6] [7] which in humans is encoded by the *afp gene* [8][9] . AFP is produced by the yolk sac and the liver during fetal life.

Like any elevated tumor marker, elevated AFP by itself is not diagnostic, only suggestive. Tumor markers are used primarily to monitor the result of a treatment (e.g. chemotherapy). If levels of AFP go down after treatment, the tumor is not growing. In the case of babies, after treatment AFP should go down faster than it would normally. A temporary increase in AFP immediately following chemotherapy may indicate not that the tumor is growing but rather that it is shrinking (and releasing AFP as the tumor cells die). AFP-L3, an isoform of AFP which binds Lens culinaris ag-

glutinin, can be particularly useful in early identification of aggressive tumors associated with hepatocellular carcinoma (HCC). AFP is the main tumor marker (sometimes with HCG) used to monitor testicular cancer, ovarian cancer, and malignant teratoma in any location: values of AFP over time can have significant effect on the treatment plan. For this reason, AFP is a valuable detection target for our FET biosensor. All AFP is purchase from Blossom Biotechnologies Inc. Taipai, Taiwan, and the all are reagent-grade quality. All the AFP samples is store in the -20 ℃.

Chapter 4 Result and Discussions

4.1 Physical and electrical properties of the back-gate SiNB-FET

The back-gated silicon nanobelt field effect transistors (NWFETs) on silicon-on-insulator wafer were successfully fabricated. The width of nanobelt is about 60nm (figure 4-1 top). It is as same as the traditional metal oxide semiconductor (MOSFETs), the values of Id can be well controlled by the applied gate voltage (Fig. 4-1(b) (c). In this case, an n-channel FET is applied a gate voltage (V_g) from negative to positive direction to induce negative charge in the channel. When the gate voltage was smaller, p-n junction was blocked the electrical current from drain to source, and there was a very low leakage current (I_{off}) in the level of picoampere (pA). When the gate voltage is high enough, construct the conducting inversion layer and 'open' the channel, the drain-to-source current (I_d) increase outstanding and the gate voltage is called 'threshold voltage (V_{th}). The threshold voltage of FET was about -1.5 V. The current (I_{on}) reach different saturation dependant on different applied drain-to-source voltage (V_d). The ON/OFF current ratio is about 5 orders of magnitude. The I_d-V_d curve also depends on controlled gate voltage (V_g), and back-gate SiNB-FET biosensors were characterized the physical and electrical properties by 4156C semiconductor analyzer.

(a)

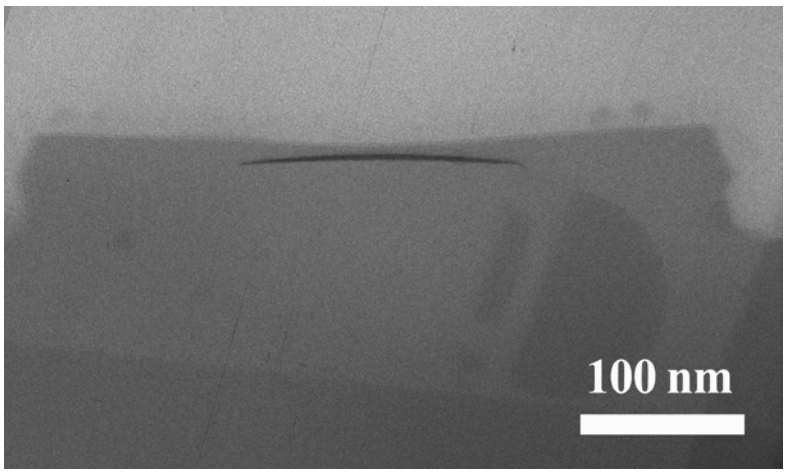

(b)

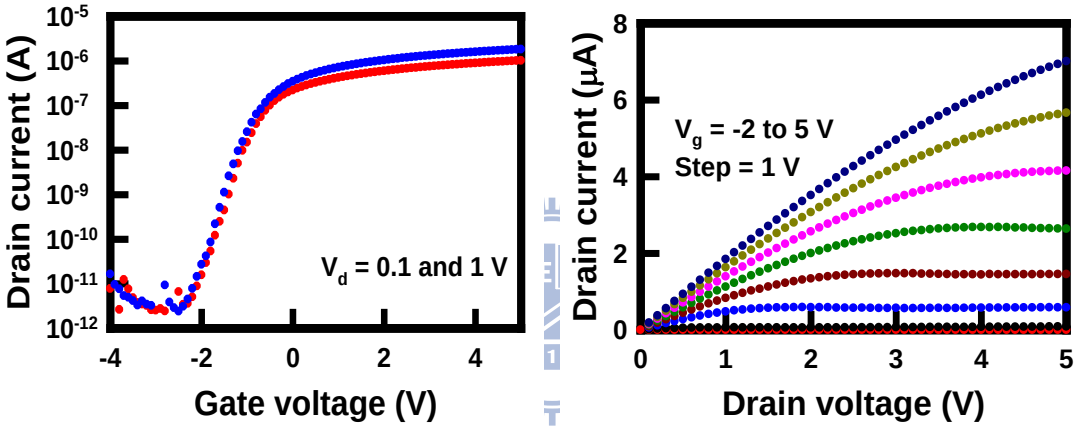

Fig. 4-1 (a) **SEM image of silicon nanobelt.** The width of nanobelt is about 60nm. (b) **Electrical properties of SiNB FET sensor**. The threshold voltage of FET we fabrication is about -1.5 V, The ON/OFF current ratio is about 5 orders. The I_d-V_d curve dependant on controllable gate voltage (V_g), and the current (I_{on}) reach different saturation dependant on different drain-to-source voltage (V_d) we applied.

4.2 Real-time Detection of the PBS pH

4.2.1 Hepatocellular carcinoma will cause blood acidosis cause

According to the reported [1], hepatocellular carcinoma (HCC) and orther cancercan alter the pH of thephysical body fluid. Because the tumor, in our paper, it stand for HCC, have a more actively and effective metabolism behavior, in order to replenish such high energy consume, more violent respiration is necessary. Such violent respiration will cause the tumor cell release more CO_2 to blood. The CO_2 in blood may enter into the erythrocyte, then converted to CO_3 by carbonic anhydrase , and release to blood. This phenomenon will cause the blood pH decrease. In addition, many different type of HCC will released AFP, this is a acidic protein (pI = 5.5), this protein also cause blood pH decreased. For these reasons, we can think the pH of blood as a indicator of health, so we want to use the bioFET to detection the pH of saline.

4.2.2 Detection response of the solution pH

Amineand oxide-functionalized SiNBs exhibit linearly pH-dependented current over a large dynamic range and could be understood in terms of the change in surface charge during protonation and deprotonation. The APTES coated process has described on previous chapter, and here we show the measurement result. At first, the PBS solution with pH 6.4 was injected to the detection region. After current was in equilibrium, the PBS solution with pH was from 6.6 to 7.4 with 0.2 in steps was then injected in sequence, and drain current of the NB FET sensor continued measuring at a constant gate voltage. As ahown in Fig. 4-2, the NB FET sensor exhibited decreasing current with the pH of solution, and the single to noise ratio was >> 3,

showing an excellent sensing ability. The drain current versus pH is shown in Fig. 4-3, which exhibits a linearly dependence over the pH 6.4 to 7.4 range. This result suggests that the NB FET could be acted as the pH sensor to screen the serum pH in the future. In previous report [2], the steady state pH sensing show the logarithmic dependence on the target molecular concentration, (in this case, target molecular is hydrogen ion). The net charge density on the sensor surface could be obtained based on first-order chemical kinetics of bond dissociation for the particular type of surface functionalization schemes was, in this case,–OH and –NH2.This is the main reason why the linear response could be obtained over a wide range of pH in our experiment.

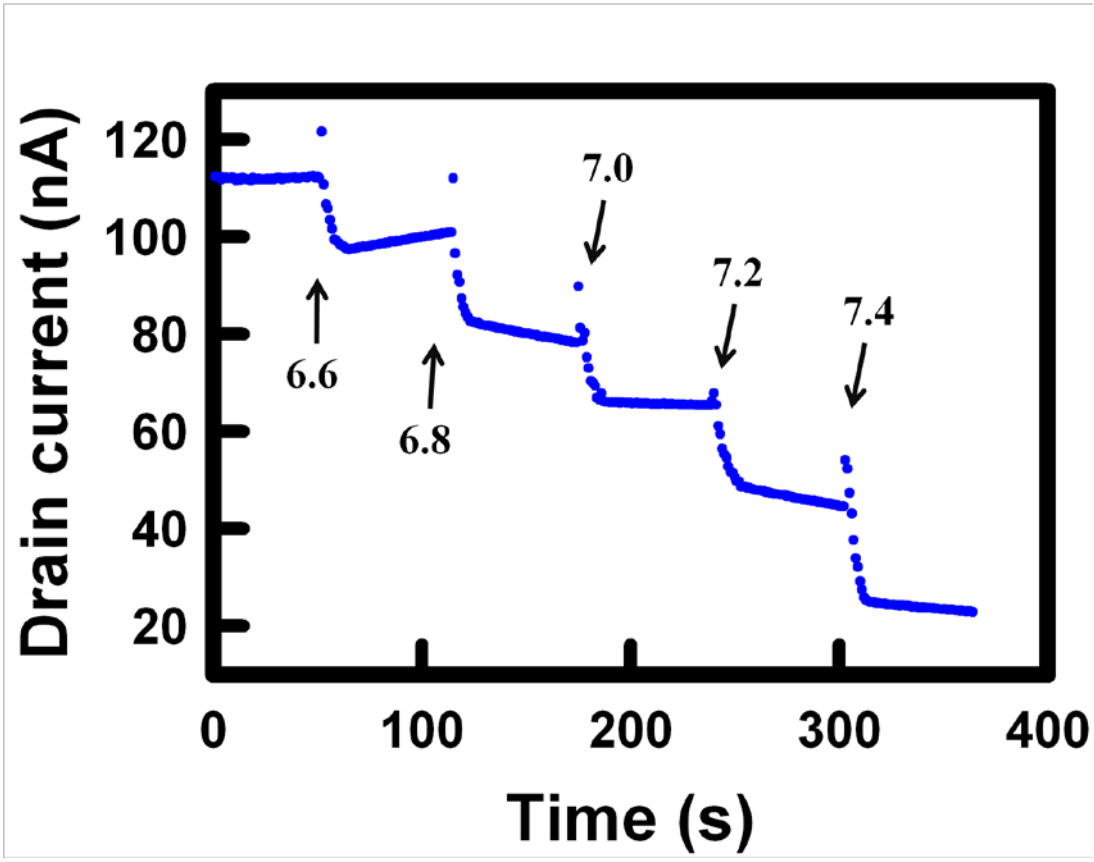

Fig. 4-2 Detecting the solution pH from 6.6 to 7.4. Drain current of sensor decreased continually dependent on the PBS we pumped, and the single /noise ratio >> 3.

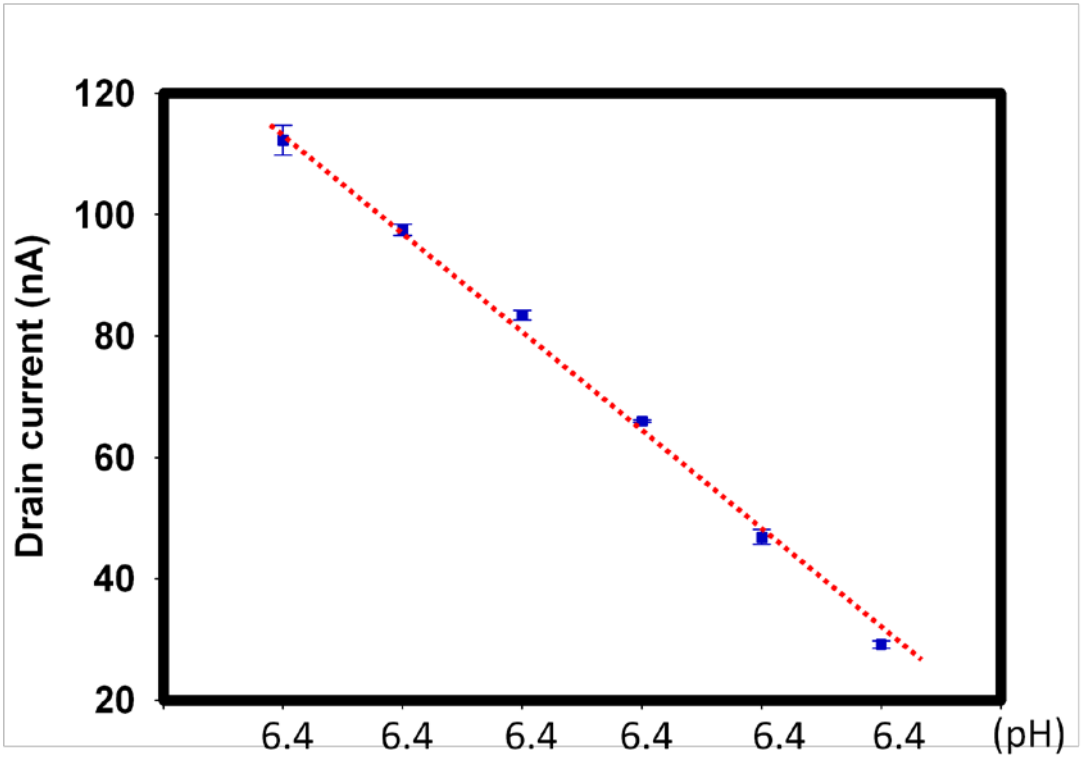

Fig. 4-3 Drain current of the NB FET sensor as a function of solution pH. Drain current and pH value has a liner relationship. The net charge density on the NB surface was obtained from charge bring chemical groups.

4.2.3 Effect of the solution ion concentration to the NBFET

The solution pH was dependent to the hydrogen ion concentration, and hence the electrical response was also correlates to the hydrogen ions concentration due to the change of surface charge. Many reports have been proposed that the ion concentration of the PBS was an important factor for bioFET sensitive. This is because that the detection of solution pH was by monitoring the bioFET drain current, which was influenced by the electrical charge of the sensor surface. Therefore, the relationship of drain current and electrical charge is dependence, and it is varied with the ion concentration of PBS.

The charge of solution-based molecules and macromolecules is screened by dissolved solution counterions: a negative species such as streptavidin or DNA will be surrounded by positively charged ions due to electrostatic interactions. On a certain length scale, termed the Debye length (ìD), the number of net positive charges approaches the number of negative charges on the protein or DNA. The result is a screening effect such that the electrostatic potential arising from charges on the pro-

tein or DNA decays exponentially toward zero with distance. Thus, for optimal sensing, the Debye length must be carefully selected for NWFET measurements because molecules binding to the devices are removed from the sensor surface by _2-12 nm. Here we reported a result to demonstrate the effect of ion concentration of PBS. We prepared PBS with three different ion concentrations, denoted 0X, 1X, and 10X, respectively. The PBS having pH from 4 to 8 was injected into the sensor, and monitored the electrical response of the bioFET sensor. The response of sensor was observed to have a relationship with ion concentration of PBS. The respond of sensor is smaller upon increasing the PBS concentration, that is, less sensitive. (Fig. 4-4)

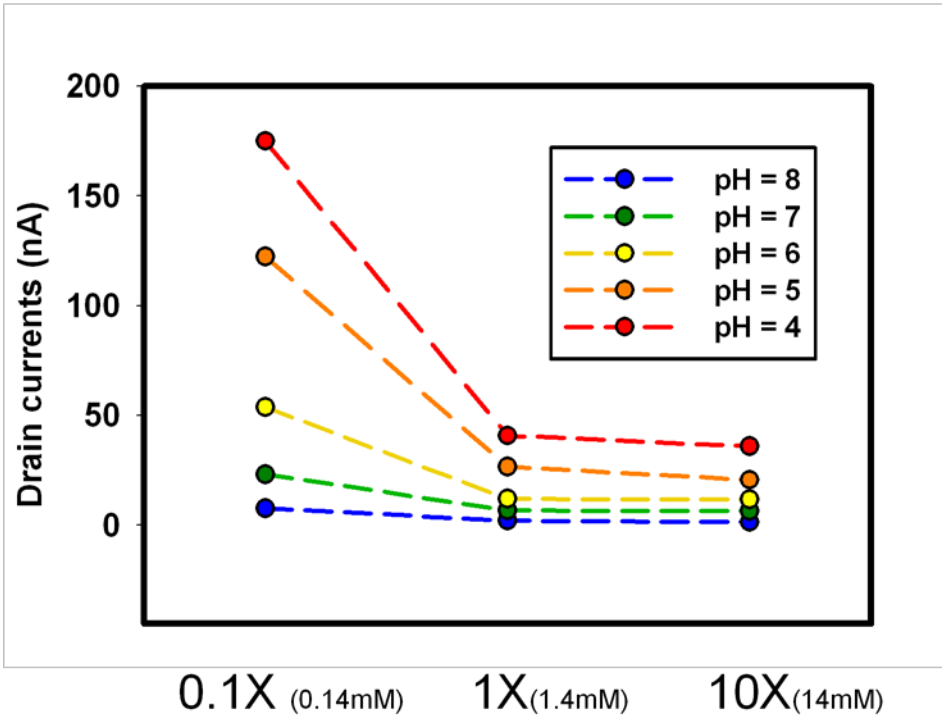

Fig. 4-4 Drain current of sensor as a function of PBS concentrations with various pH solution. Concentrated of the PBS, the respond of sensor is decrease. Three different ion concentrations PBS, there are 0.X, 1X, and 10X respectivity. And we pumped pH value 4 to 8 PBS, in the figure are use different colors to express.

4.3 Real-time detection of HBV x gene fragments

4.3.1 Certification of DNA immobilization by fluorescence image

In order to confirm successful immobilization, DNA with a fluorescence labeled in the 3’ terminal was employed. We used the fluorescence microscope to observe the DNA immobilization. Figure 4-5 shows the fluorescence image of the fluorescence-labeled DNA immobilized on the 60 nmsilicon nanobelt. This is a strong proof to demonstrate the DNA exactly immobilized on the silicon nanobelt.

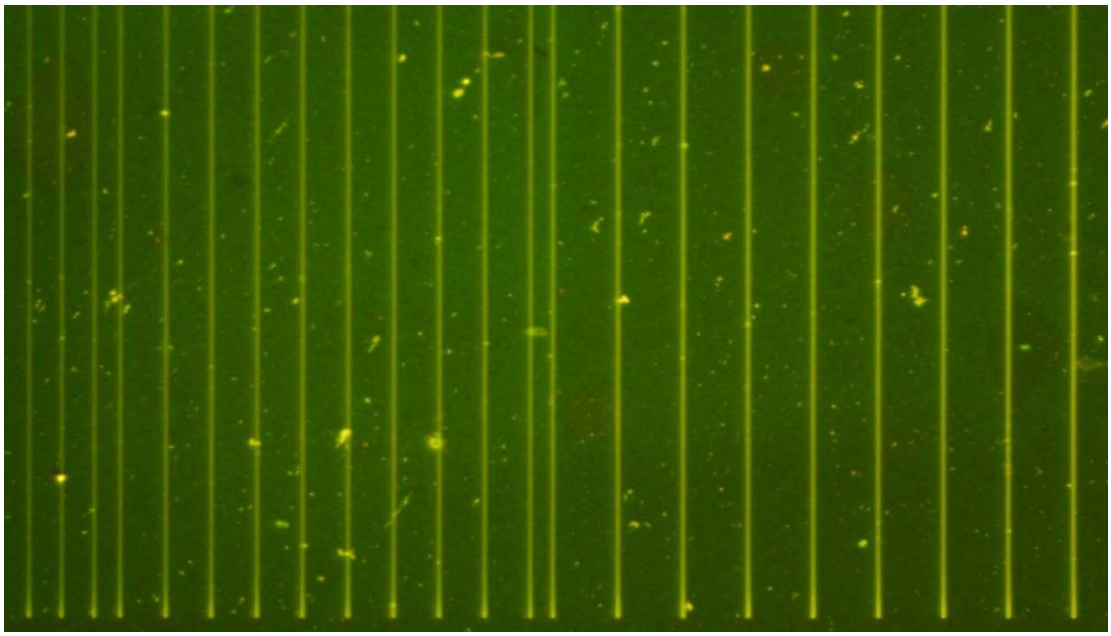

Fig. 4-5 Fluorescence image of the fluorescence-labeled DNA immobilized on the 60 nm-silicon nanobelt. The DNA which functional fluorescence compound in its 3’ end. We use the fluorescence microscope to confirm the immobilized situation.

4.3.2 Effect of PBS to the bioFET DNA sensor

The ions in PBS have the potential to influence the response of FET biosensor. This phenomenon may cause a bed result of sensing, for example false positive or false negative. Figure 4-6 is the experiment result to prior rectify the phosphate ef-

fect to our bioFET DNA sensor. A pick will appearance and following slight drain current decrease when the PBS path through the sensing zone of bioFET DNA sensor. (The drain current value has about 4 percent decreased)

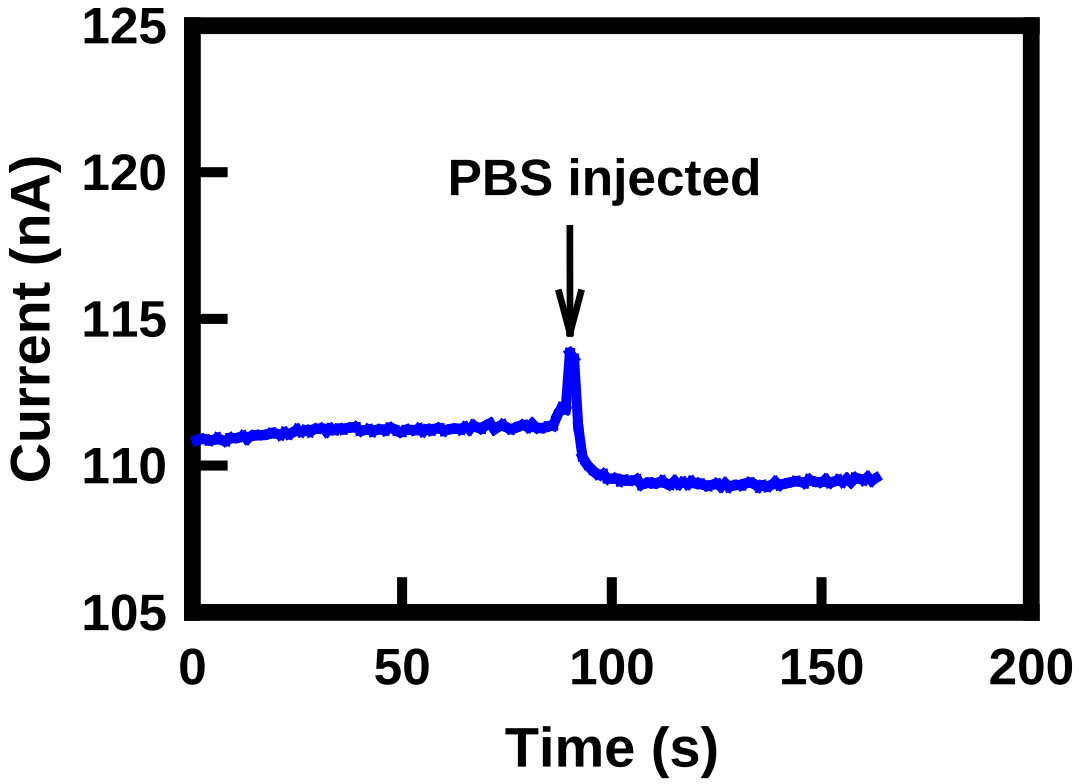

Fig. 4-6 Typical electrical response of PBS injection into the BioFET sensor. Drain current value has about 4 percent decreased, this would caused by silicon oxide and bare APTES coated on the sensing zone.

4.3.3 Real-time detection of X gene DNA fragments with various concentrations

In this section, HBV X gene DNA fragments with various concentrations including 1fM, 10fM, 100fM, and 1pM, was injected into the sensor and monitored their responses.The relationship between DNA concentration and drain current was shown in Fig. 4-7. The more concentrate DNA solution injected into the sensor, the more drain current decreased was monitored. This result was caused by the high

level negative charge contained in the DNA sequence. The increased negative charge hindered the conducting channel of bioFET DNA sensor, and hence decreased the drain current.

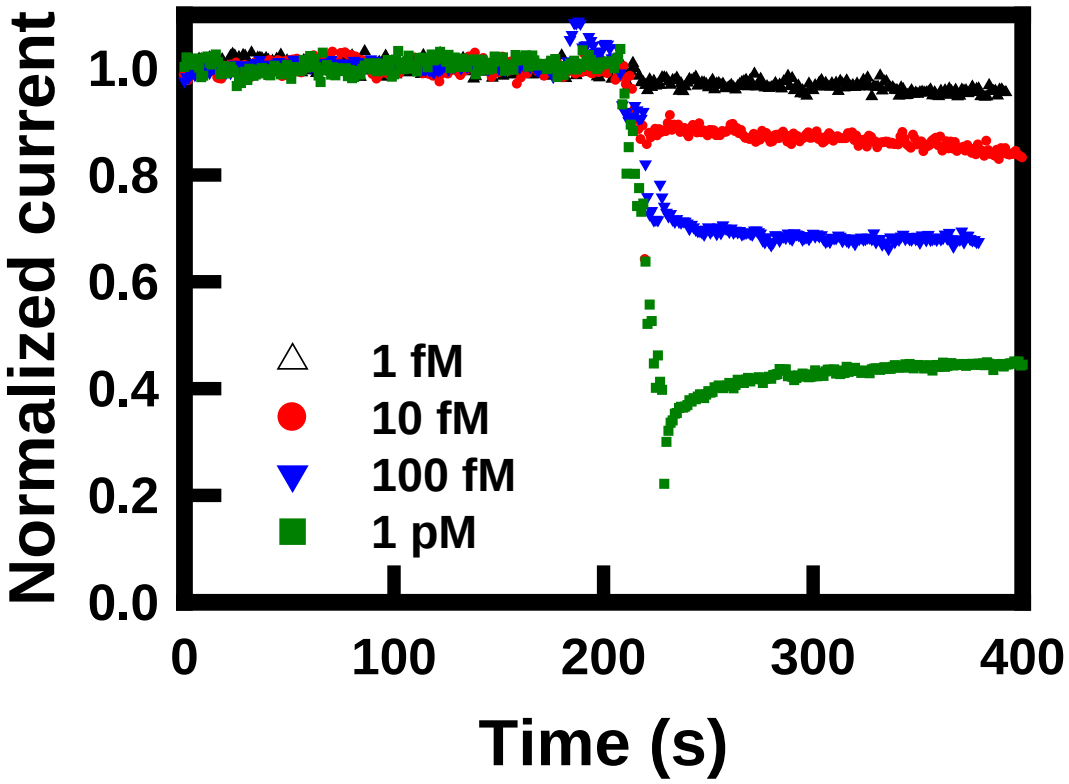

Fig. 4-7 Electrical responses of HBV X gene DNA sample with various concentrations. 1pM sample has about 70% drain current decreasing (green), 100fM sample has about 39% drain current decreasing (blue), 10fM sample has about 10% drain current decreasing (red), and 1fM sample has about 5% drain current decreasing (black), but the 1fM sample result is less statistic significance. In the end, we also test the specificity of our bioFET DNA sensor

4.3.4 Determination the sensing limit of bioFET DNA sansor

The normalized current shift exhibits a good linearity with logarithmic DNA concentration (Figure 4-8). The linear fitting for the calibration curve is y = 0.2105* log

(x) - 0.088, with a correlation coefficient of 0.9926. The detection limit of this bio-sensor, which is defined as DNA concentration that gives a signal intensity which is 3 times the standard deviation of the blank, is estimated to be 2.4 fM. This result demonstrated that our sensor is potential in diagnosing HBV because of its excellent senssitivity.

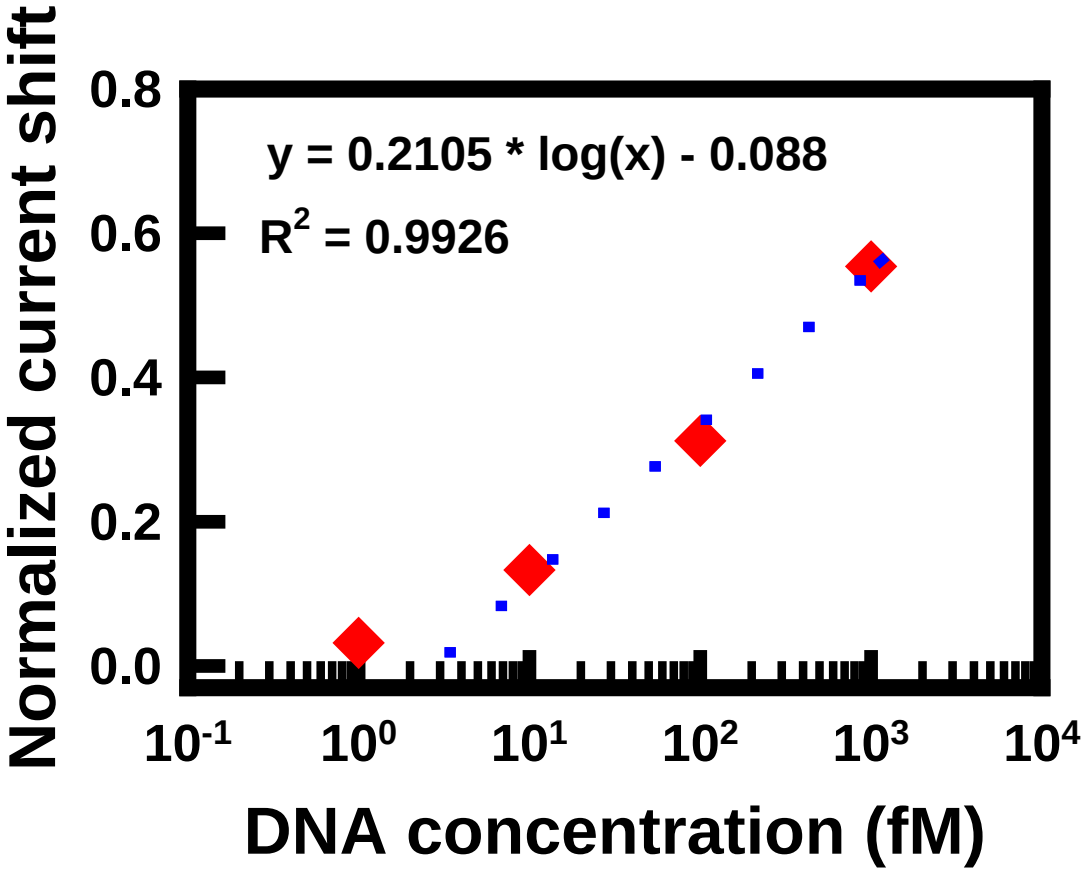

Fig. 4-8 Detection limit of the DNA sensor. The detection limit is very close to 1fM level, and the detection range of detection is about four orders.

4.3.5 Determination of the specificity sensing

Two important factors are most concerned in fabricating a good sensor. In the prior section, we demonstrated the sensitivity of our sensor. In this section, the property of specific binding was examined. The specificity is a essential topic and a big challenge of sensing technology. In faced, most of all sensors, no matter what molecules they sense sensing, encountered the false-positive problem. We employed various sequences of DNA fragments, including 1-base, 5-bases, and all-bases mis-match DNA fragments, to demonstrate the specificity property of the sensor. Figure 4-9 shows the electrical responses of the mismatch DNA injected into the NB sensor. The black curve is the control sample of HBV X gene DNA fragment (complemen-tary), and the current was decreased largely. The current shifts of 5-bases and 15-bases mismatched target DNA are almost invisible, while the 1-base mismatched sample exhibited a current decrease. This result implies the 1-base mismatched tar-get DNA nonspecific binds to the capture DNA probe in a small quantity, but the difference can be distinguished from the complementary sample. Similar result has been reported that the 3-mismatched mutant genes were nonspecific interaction to the nanowire sensor but can be quantified and distinguished from the wild type genes.

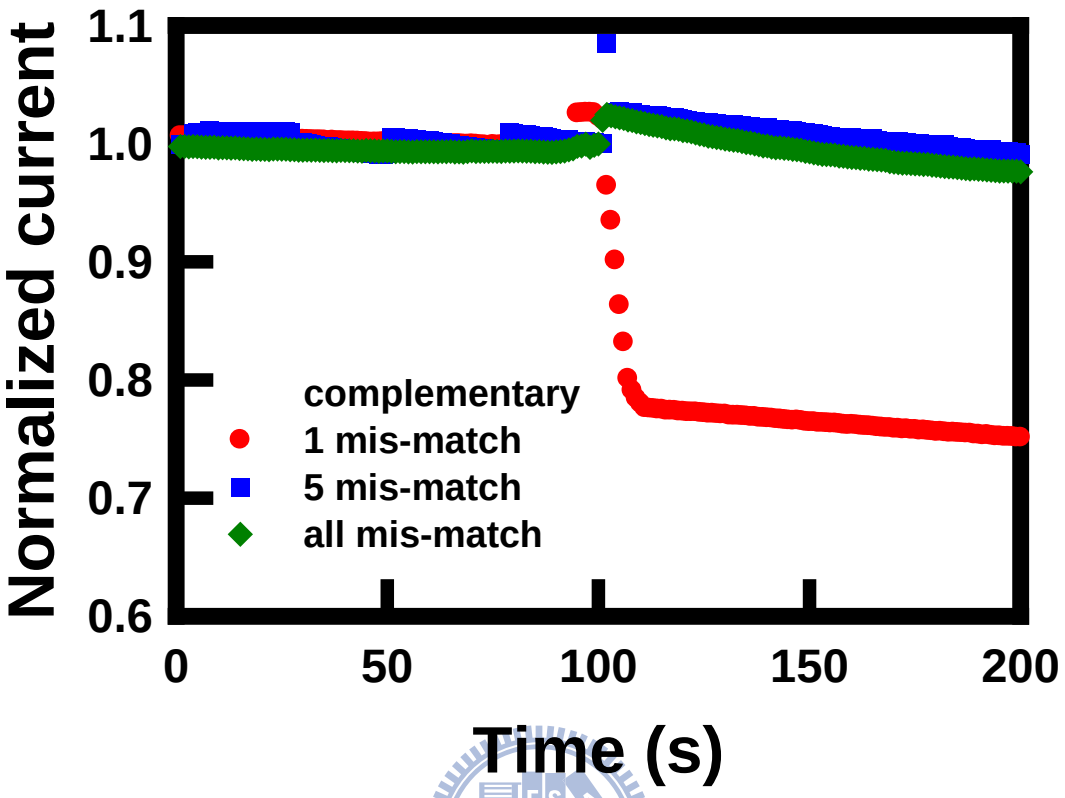

Fig. 4-9 Response of the mismatch DNA of the DNA sensor. Detection response of complementary, and 1-base, 5-bases, and 15-bases mismatched target DNA samples. DNA sensor has no response to all of bases mismatch (green curve) and five bases (blue curve) mismatch. DNA sensor can distinguish just one mismatch DNA fragments. (red curve), compared to the complementary sequence, the drain current of one mismatch sequence is about ten percent higher.

4.4 Real-time detection of the liver cancer maker AFP

4.4.1 Detection the different concentration AFP DNA fragments sample solution

AFP (AFP, α-fetoprotein) is a protein [7][8], synthesis by the yolk sac and the liver during fetal life. In humans, AFP produce levels decrease gradually after birth, reaching adult levels by eight to twelve months. Normal adult alpha-fatoprotein levels are low, but still detectable. In normal, alpha fetoprotein has no obvious function, and the level maintain in a steady-state, but like other elevated cancer maker, it is a index for the program of hepatocyte tumor or liver cancer. When the health of liver goes to worsen, the AFP level would increase. On the contrary, if level of AFP goes down after treatment, the tumor is not growing. For these reasons, we chose AFP as the target molecular for trace the aggressive of liver cancer. In figure 4-10, we coated the anti-AFP antibody on the sensing zone of our bioFET, which is specific captured to the AFP. Because AFP carries negative charges, the drain current will decrease when alpha fetoprotein is captured on the detection region. We prepared 3 ng/ml (black circle), 15 ng/ml (red triangle), 30 ng/ml (blue square), 50 ng/ml (green triangle), 100 ng/ml (brown square), 300 ng/ml (light blue crucifix), and 600 ng/ml (olive green hexagon), and we can see that there is a relationship between drain current value and concentration of AFP. Figure 4-10 also shows our bioDET AFP sensor can be saturated when the concentration of alpha feto-protein is higher than 100 ng/ml, hence the detection range of our bioFET AFP sensor is about two orders. In figure 4-11 we can see the current value and AFP concentration are logarithmic dependent, except the two saturated concentration level.

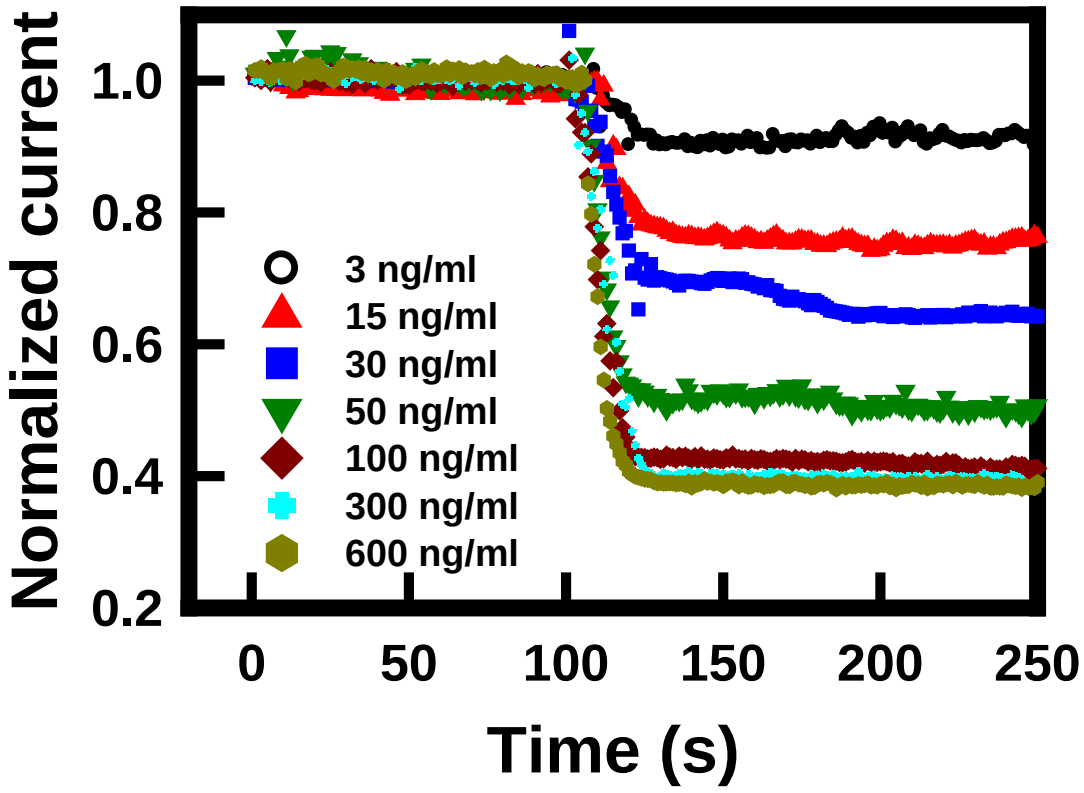

Fig. 4-10 Detection response with various AFP concentrations from 3 to 600 ng/ml. The drain current decreased level is dependent on the AFP concentration in the sample solution.

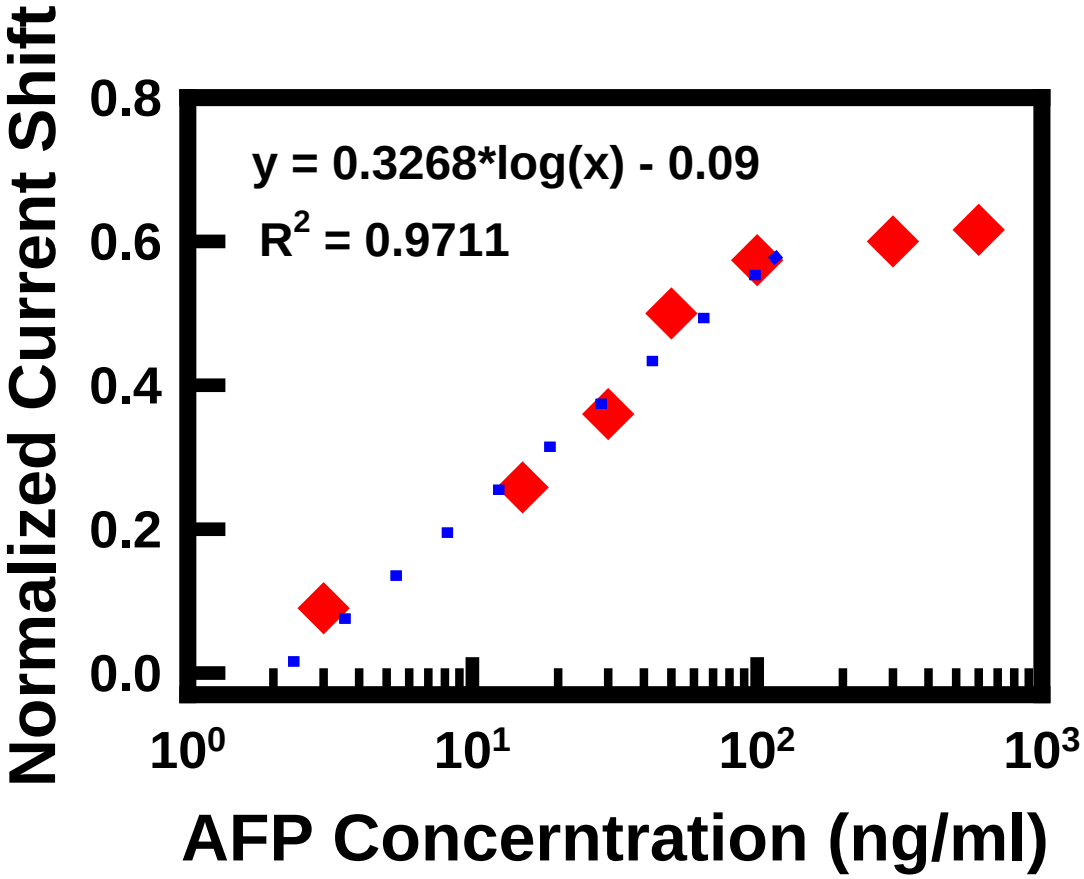

Fig. 4-11 Normalized current shift as a function of AFP concentration. The drain current value of bioFET AFP sensor and AFP concentration are logarithmic dependent, except the two saturated concentration level.

4.4.2 Detection the real mouse AFP level

Blood plasma is not like PBS, the plasma contained a good deal of DNA, RNA, protein, and several other compounds. These impurities, in generally, influence or obstruct the sensitivity and specificity of biosensor by erode, block, destroy, capping, nonspecific binding, or change the electrical properties of biosnesor. Therefore, the detection result of biosensor may have a significant difference between targeting molecular which dissolve in PBS and in its physiology environment. For this reason, we also detected AFP level in the real mice. In figure 4-12, because the

AFP level is not the same [9] [10] in the infant mice and adult mice, the drain current decrease level is different. The adult mice AFP sample decreased the drain current value about twenty percent, while forty percent for the infant mice AFP sample. Compare to the figure 4-8, the AFP level of adult and infant mice, was estimated to be about 15 and 50ng/ml, respectively. We picked this result to contrary to literature which study the value about mice [11-16], and foung the AFP level of real mice was very similar to that of in PBS. This result indicates the influence of impurity is not very obvious in our bioFET AFP sensor.

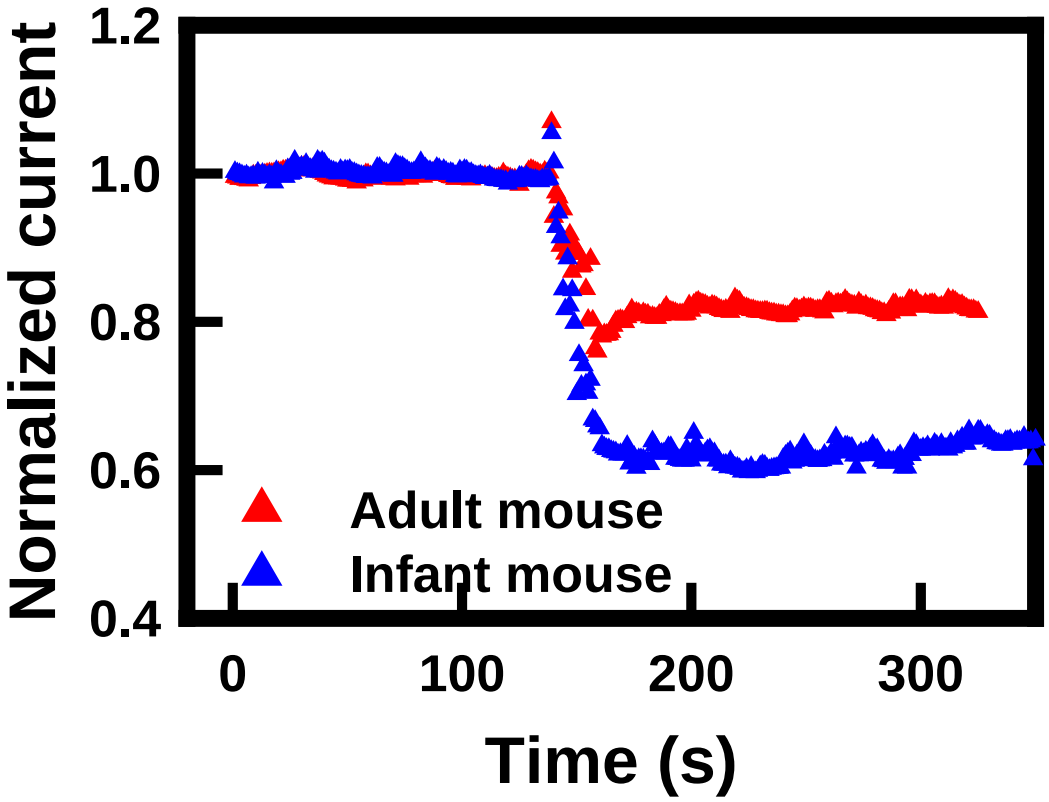

Fig. 4-12 Detecting response of AFP concentration from adult and infant mice. The AFP level of adult mice and baby mice, is about 15ng/ml, and 50ng/ml, and cause the drain current decrease 20% and 40 %, respectively.

4.4.3 Real-time detection of the AFP with various PBS concentrations

The relationship of drain current and electrical charge there are not always in constant, it's varied with ion concentration of PBS. Because of within the ion concentration charge, the debye length change, and this phenomenon decide the ability of sensing of our bioFET DNA sensor. Figure 4-13 shows the influence of PBS ion concentration by our sensor detection. The PBS with 10X, 2X, 1X, and 0.1X in concentrations was injected into the sensor in sequence. As shown in Fig. 4-13, the bioFET AFP sensor in10X PBS environment was less sensitive, and the bioFET AFP sensor in 0.1X PBS was the most sensitive. The relationship between drain current change and PBS was logarithmic dependence. This result is consistent to other study [17], and intuitively obvious because screening by the ions suppresses the overall charge effective in modulating the sensor response. The results also show that optimizing the ion concentration of PBS in experiments is the critical importance in studying biosensors, because the same target molecules might result in different sensitivity with different concentration electrolyte.

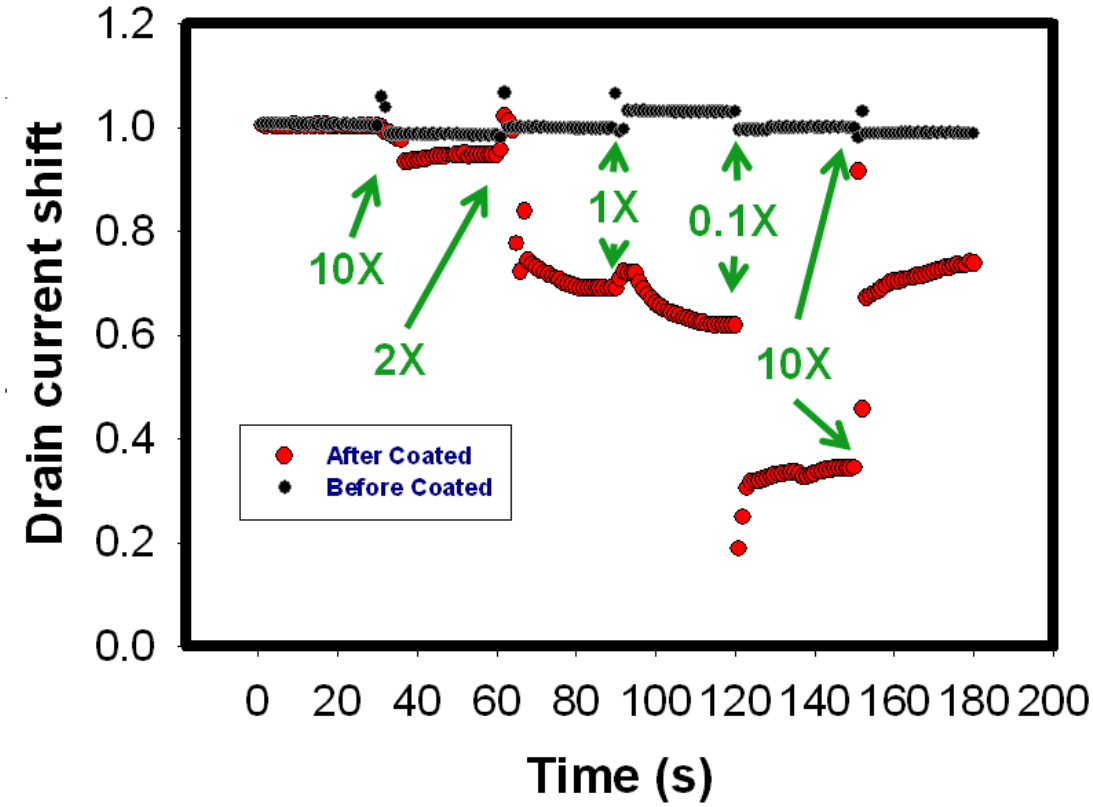

Fig. 4-13 Influence of PBS ion concentration by our sensor detection. We prepared the 10X, 2X, 1X, 0.1X PBS, and we pumped 10X, 2X, 1X, 0.1X, and back to 10X PBS in sequence. And monitor the drain current value. As the result, we can see the bioFET AFP sensor in10X PBS environment is most less sensitivity , and the bioFET AFP sensor in 0.1X PBS is most sensitivity. And the relationship between drain current change and PBS is logarithmic dependent.

4.5 Life time identification of the self-assembled monolayer

4.5.1 Identification of the ion impurities trapped in SOI wafer

In previous experiments described above we used PBS as buffer solution, the PBS buffer was,however, might contain problems. The PBS solution contained sodium ions, which was reported to affect device performance due to ions trapping phenomenon into the silicon.[18]. The sodium ions might alter or destroy the crystal lattice, resulting in current decreased and unstable of the device. Here we reported the experimental result of the electrical performance about the PBS soaped effect, which was caused by the sodium ions in the PBS buffer. As shown in the Figure 4-13, the current was increased dramatically after 0.5 day PBS soaping, which might be caused by the diffusion of sodium ions into oxide film. This result was similar to the well-known mobile ion charge trapped in the oxide film, resulting in the left-shift of the I_D-V_G curve. Therefore, The drain current was increased as biased at a constant gate voltage. After two day immersing, the drain current was continuously decreased with days. In addition, the decreased current ratio of the sensor was dependant to the PBS concentration. This result illustrated that the current path of the NB FET was obstructed by the sodium ions.

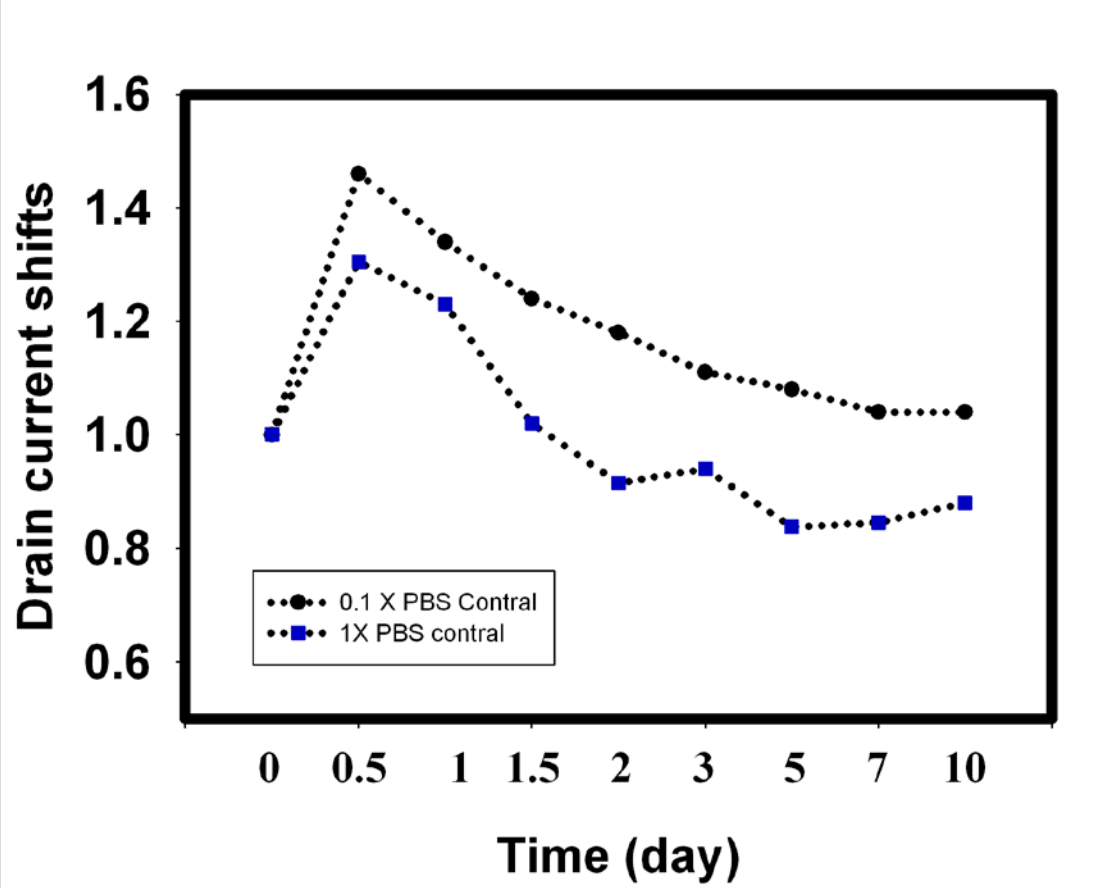

Fig.4-14 Drain current shifts of the NB FET sensors as a function of PBS soaping days. The prior increase drain current caused is by the parallel currents through PBS solution. After 0.5 days and later, drain current decreased as the daytime increase. And high level ion concentration causes the drain current degeneration much serious. It believed caused by more sodium ion trapping into the SOI wafer crystal lattice.

4.5.2 Duration of APTES film on silicon oxide by AFM examination

The intact of self assembled monolayer on the bioFET sensor detection region (in our case includeed APTES, HBV X gene complementary DNA, and AFP) is a critical factor in concerning to the sensitivity and specificity. Unfortunately, instead of the permanence of these self-assembled monolayers on silicon oxide film, they degenerate with time. Here we used AFM to monitor the life time of APTES

self-assembled monolayer coated on silicon oxide. As Figure 4-15shows, there is no obviously difference between 0 and 12 hours soaping, while the morphology of APTES film started to aggregate after 36 hours soaping, implying that the APTES film was destroyed and crystallized.

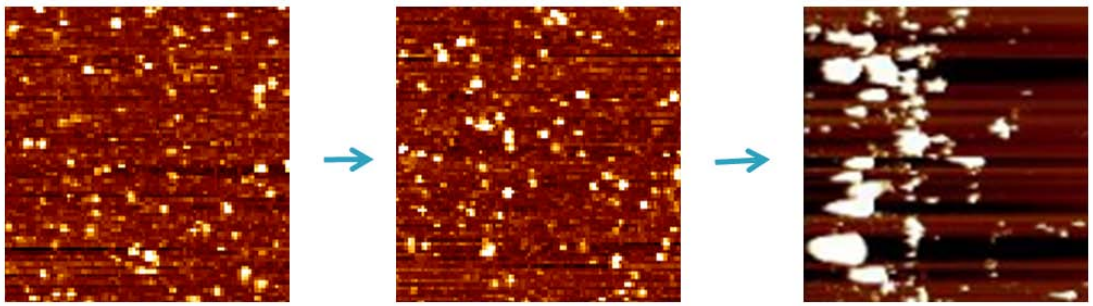

Fig. 4-15 AFM images of APTES self assembled monolayer after various soaping time. No obviously difference during 0 hour to 12 hours. After thirty-six hours, the APTES film look like to crystallize and the self-assemble film seen is destroyed.

4.5.3 Duration of DNA strand on silicon oxide

In section 4.5.2, we have demonstrated that the APTES film degenerated with time, and this degeneration procedure was accelerated by PBS soaping. In this section, we monitored the current shift of BioFET DNA sensor to further demonstrate the degeneration phenomenon.

First, a 15-mer DNA strand was immobilized on the sensor surface by APTES linker. Because the macromolecule of DNA bore lots of negative charges, the existence of DNA could be served as a molecular amplified to electrical signal. Figure 4-16 illustrates the current shift of samples as a function of soaping time. The black curves were the control sample, which the sensor surface was before any modificai-

ton.. The drain current decreased might be caused by Na^+ trapping into the crystal lattice of silicon nanobelt; the green curves were the NB FET sensors modified by APTES on the detection region, and the decreased of drain current was possibly caused by two factor, (1) by Na^+ trapping, and (2) the degeneration of APTES. The reason of (2) is because the sensor was soaped in a buffer solution with pH 7.4, and APTES bore positive charges in this environment, the conduct of BioFET was hence increased. Once the APTES film started to degenerate, the positive charges on the detection region were decreased, resulted in a decreasing of the channel conductivity. The sensors with DNA immobilized on the surface were shown as the red curves, and the drain currents were increased with soaping time. We believed that this phenomenon was caused by the Na^+ trapping effect to the field effect of sensor. Because the negative charge carried on DNA caused the drain current decreased, once the DNA molecules stared to degenerate, the drain current was increased. Moreover, the current that sensor soaped in 0.1X PBS was different to that in 1X PBS. this phenomenon was believed to cause by different debye length and degeneration rate with different concentrations of the solution.

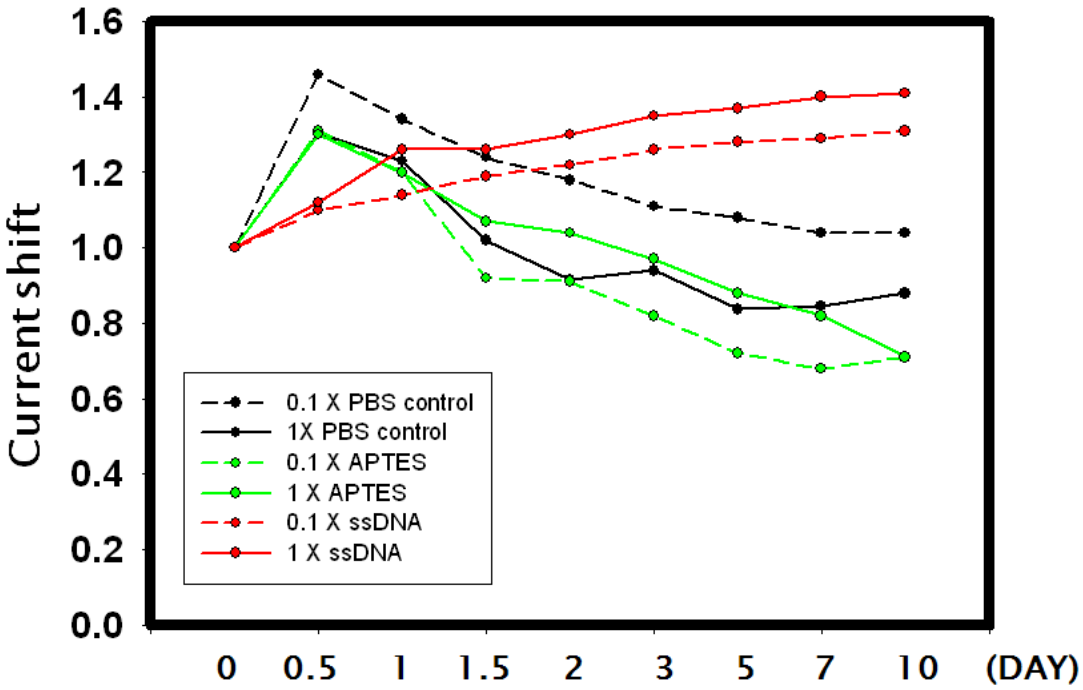

Fig. 4-16 Current shift of the modified NB FET sensor with soaping time. The black curves set as control, Drain current decreased may cause by Na^+ trapping. The green curves are the FET, drain current decreased caused by Na^+ trapping, and the degeneration of APTES SAM; Red curve is coated DNA, drain current of these increased That believedcaused by Na^+ trapping effect counteract to the field effect of negative charge of DNA. Dotted line are sample soaped in 0.1X PBS, drain current variation level is also will influenced by different ion concentration of PBS.

4.5.4 The degeration mechanism of self-assembled APTES monolayer on silicon oxide surface

The APTES modified to the silicon oxide was by the silanization interaction. The hydroxyl group on silicon oxide and the ethanol group was covalent binding, and released three ethanol molecules (three silanization reaction for one APTES with silicon oxide surface). The three ethanol groups of APTES not always react completely with hydroxyl group of silicon oxide (figure 4-17, (a)). Furthermore, the silanization is a reversible chemical react, hence the APTES may peel off from silicon

oxide surface. The peeling-off APTES film remained free ethanol group (which has no silanization with silicon oxide hydroxyl group) react with APTES which ethanol group is leaving (Figure 4-17 (b)), forming a compound which has two APTES molecular combined by ether bond, and an ethanol group leave (Figure 4-17(c)). Finally the diAPTES compound will stack in a regular pattern and crystallize (Figure 4-17 (d)). The resulting morphology measured by AFM was shown in the bottom of Figure 4-17.

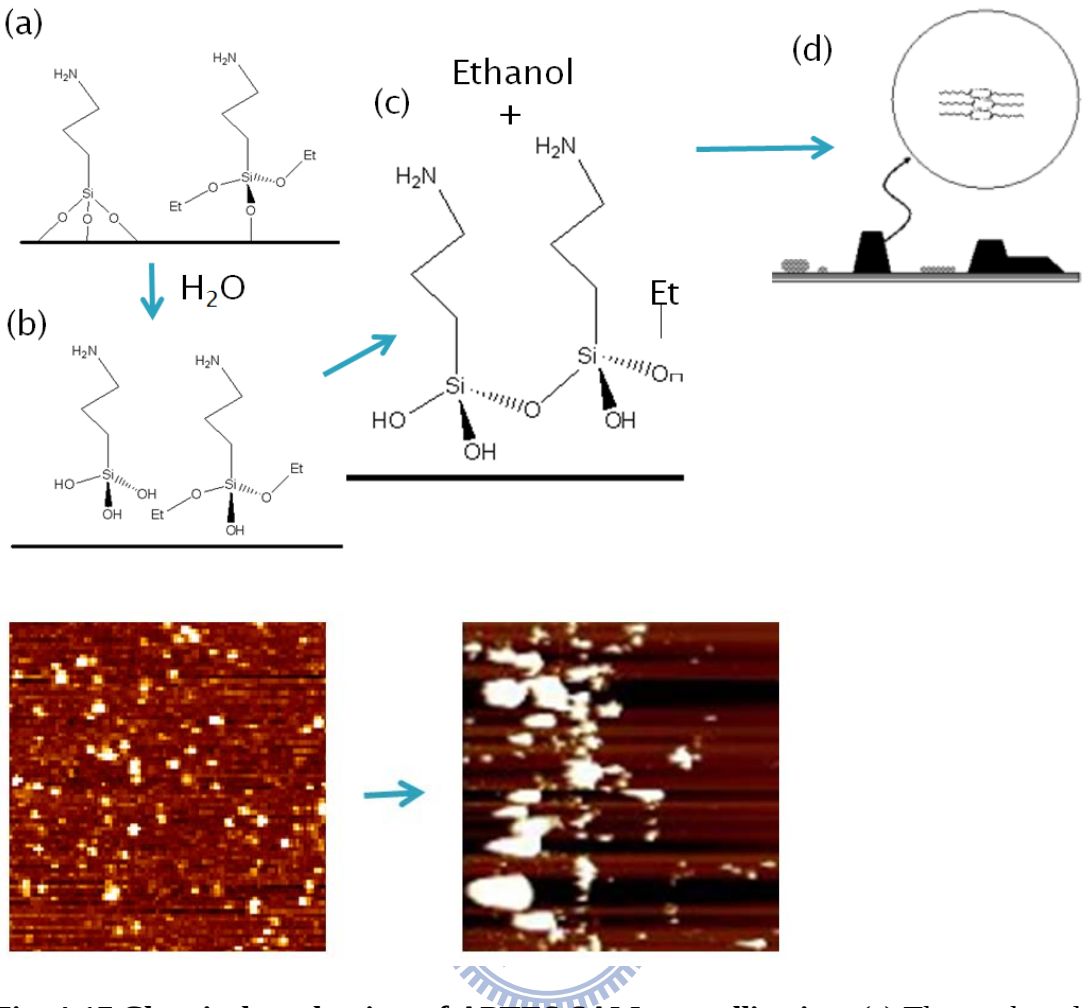

Fig. 4-17 Chemical mechanism of APTES SAM crystallization. (a) Three ethanol group of APTRS are not always complete reaction with hydroxyl group of silicon oxide(b) silanization reaction is a reversible chemical reaction. (c) APTES which fall off from the silicon oxide surface will covalent binding, forming a compound which has two APTES molecular combined by ether bond.

Chapter 5 Conclusion

We have demonstrated a novel back-gate SiNB-FET for real-time sensing of solution pH, HBV X gene, and AFP cancer marker. The SiNB-FET was fabricated by integrating the conventional top-down CMOS compatible-SiNB-FET technology, including the LOCOS isolation process and the shrinking nanobelt with higher surface-to-volume ratio. The back-gate device provides a good quality of gate dielectric, which exhibits a very low leakage current and excellent field effect property. The width and thickness of shrank nano-channel can be down to 150 and 5 nm, respectively. The electrical characteristic of the SiNB-FET exhibited five orders of magnitude on I_{on}/I_{off}. For pH sensing, SiNB-FET pH sensor can distinguish pH value between pH6.4 to pH7.4 in 0.2 step. The sensitivity of pH sensor was influenced by the ion concentration of PBS. Low concentration PBS will enhance the sensing ability of the sensor. We successfully detected the X gene DNA fragments by the SiNB FET sensor, and the concentration could be down to 10 fM. We also tested the specificity the sensor, and the highly specificity even one-base mismatch DNA strand could be distinguished by the sensor. The HCC related AFP cancer marker was also detected by the NBFET sensor. By tunning the applied gate voltage, the SiNB-FET could detect the AFP in ng/ml level. The serum AFP was also detected from real mice, and the results showed low influence of impurity in the mice blood plasma. Our approach offers the possibility of highly parallel detection of multiple chemical and biological species, as well as for monitoring real-time response in a single integrated chip in the future. An improvement in our study, in terms of sensitivity and reliability of the real-time recordings could be done well by using in-vitro biomolecule assays, where the DNA hybridization reaction and antibody interaction with antigen are achieved in a liquid environment by microfluidic system being used

for real-time, label-free recording.

Reference:

Chapter 1

[1] G. M. Whitesides, J. C. Love, *Sci. Am.*, **2001**, *285*, 38

[2] D. Mijatovic, J. C. T. Eijkel and A. van den Berg, *Lab Chip*, **2005**, *5*, 492

[3] H. V. Jansen, N. R. Tas and J. W. Berenschot, *Encyclopedia of Nanoscience and Nanotechnology, ed. H. S. Nalwa*, **2004**, *5*, 163

[4] P. Mela, N. R. Tas, A. van den Berg and J. E. ten Elshof, *Encyclopedia of Nanoscience and Nanotechnology, ed. H. S. Nalwa*, **2004**, *6*, 739

[5] S. A. Gajar and M. W. Geis, J. *Electrochem. Soc.*, **1992**, *139*, 2883.

[6] National Science Foundation. (http://www.nano.gov/)

[7] H.zhu, and M.Snyder, *Current opinion in chemical biology*, **2003**, *7*, 1.

[8] E.Souteyrand, J.P.Cloarec, J.R. Martin, C.Wilson, I.Lawrence, S.Mikkelsen, and M.F.Lawrence, *J. Phys. Chem. B*, **1997**, *101*, 2980.

[9] P.Bergveld, *Sensors and Actuators*, **1985**, *8*, 109.

[10] A.Miller, F.K.Perkins, M.Peckerar, S.fertig, and L.Tender, *Circuits and Systems, 2003. ISCAS '03. Proceedings of the 2003 International Symposium on*, **2003**, *3*, III-918

[11] T.Senda, S.Wakamatsu, A.Nakasa, U.Akiba, M.Fujihira, *Unltramicroscopy*, **2003**, *97*, 1-4, 27.

[12] K. Y. Park, M. S. Kim, K. M. Park, and S. Y. Choi, *Electrochemical Society*, **2006**, 206.

[13] D. K. Schwartz, *Annu. Rev. Phys. Chem.*, **2001**, *52*, 107.

[14] F. Herelle Res., *Microbiol.*, **2007**, *158*, 553–4

[15] C. Papadopulos, B. H. Chang, A. J. Yin, J. M. Xu, Int. J. *Nanoscience*, **2002**, *1*, 205.

[16] E. J. Bae, W. B. Choi, K. S. Jeong, J. U. Chu, G. S. Park, S. Song, K. Yoo, *Adv. Matter.*, **2002**, *14*, 277.

[17] T. B. Tomasi, *Annual review of medicine*, **1977**, *28*, 453

[18] G. J. Mizejewski, *Experimental biology and medicine*, **2001**, *226*, 377

[19] M. E. Harper, A. Dugaiczyk, *American journal of human genetics*, **1983**, *35*, 565

[20] NCBI, Entrez Gene: AFP (http://0rz.tw/umYg8)

[21] Y. Binghui, Z. Boheng, X. Yaochao, W. Wenping, S. Yuefang, Z. Anru, X. Zhong, *J. Cancer Res Clin Oncol*, **1997**, *123*, 357

[22] K. Okuda, *J. Hepatology*, **2000**, *32*, 225

[23] C. C. Harris, *Toxicology Letters*, **1995**, *82-3*, 1

Chapter 2

[1] D. Olmos, A. J. Aznar,J. Baselga, J. Gonzalez-Benito, *J. Colloid Interface Sci.*, **2003**, *267*, 117

[2] R. Albala, D. Olmos, A. J. Aznar, J. Baselga, J. Gonzalez-Benito, *J. Colloid Interface Sci.*, **2004**, *277*, 71

[3] H. Watson, A. Norstrom, A. Torrkulla,J. Rosenholm, *J. Colloid Interface Sci.*, **2001**, *238*, 136

[4] B. Wang, Y. Huang, L. Liu, *J. Mater. Sci,*. **2006**, *41*, 1243

[5] D. Enders, T. Nagao, A. Pucci, Nakayama,T. *Surf., Sci.*, **2006**, *600*, 71

[6] E. S. Kooij, E. A. M. Brouwer,H. Wormeester, B. Poelsema, *Langmuir* **2002**, *18*, 7677-7682

[7] D. Enders, T. Nagao, A. Pucci, T. Nakayama, *Surf. Sci*. **2006**, *600*, 71

[8] E. S. Kooij, E. A. M. Brouwer,H. Wormeester, B. Poelsema, *Langmuir*, **2002**, *18*,

7677

[9] K. E. Sapsford, F. S. Ligler, *Biosens. Bioelectron*. **2004**, *19*, 1045

[10] Balasundaram, G.; Sato, M.; Webster, *T. J. Biomaterials* **2006**, *27*, 2798

[11] H. Tang, W. Zhang, P. Geng, Q. Wang, L. Jin, Z. Wu, M. Lou, *Anal. Chim. Acta*, **2006**, *562*, 190

[12] T. Nakagawa, T. Tanaka, D. Niwa, T. Osaka, H. Takeyama, T. Matsunaga, *J. Biotechnol.* **2005**, *116*, 105

[13] J. K. Kim, D. S. Shin, W. J. Chung, K. H. Jang, K. N. Lee, Y. K. Kim, Y. S. Lee, *Colloids Surf., B: Biointerfaces*, **2004**, *33*, 67

[14] S. C.Jain, V. K. Tanwar, V. Dixit, S. P. Verma, S. B. Samanta, *Appl. Surf. Sci.* **2001**, *182*, 350

[15] E. T. Vandenberg, L. Bertilsson, B. Liedberg, K. Uvdal, R. Erlandsson, H. Elwing, I. Lundstroem, *J. Colloid Interface Sci.* **1991**, *147*, 103

[16] D. Kowalczyk, S. Slomkowski, M. M. Chehimi, M. Delamar, *Int. J. Adhes. Adhes,* **1996**, *16*, 227

[17] A. Simon, T. Cohen-Bouhacina, M. C. Porte, J. P. Aime, C. J. Baquey, *Colloid Interface Sci.*, **2002**, *251*, 278

[18] M. Etienne, A. Walcarius, *Talanta,* **2003**, *59*, 1173

[19] D. F. Siqueira Petri, G. Wenz, P. Schunk, T. Schimmel, *Langmuir,* **1999**, *15*, 4520

[20] S. Flink, F. C. J. M. Van Veggel, D. N. Reinhoudt, *J. Phys. Org. Chem.* **2001**, *14*, 407

[21] A. A. Golub, A. I. Zubenko, B. V. Zhmud, *J. Colloid Interface Sci.*, **1996**, *179*, 482

[22] K. M. R. Kallury, P. M. Macdonald, M. Thompson, *Langmuir*, **1994**, *10*, 492

[23] P. Silberzan, L. Leger, D. Ausserre, J. Benattar, J. *Langmuir*, **1991**, *7*, 1647

[24] E. T. Vandenberg, L. Bertilsson, B. Liedberg, K. Uvdal, R. Erlandsson, H. Elwing, I. Lundstroem, *J. Colloid Interface Sci.* **1991**, *147*, 103-118

[25] M. E. McGovern, K. M. R. Kallury, M. Thompson, *Langmuir*, **1994**, *10*, 3607.

[26] P.Silberzan, L. Leger, D. Ausserre, J. Benattar, *Langmuir*, **1991**, *7*, 1647.

[27] D. L. Angst, G. W. Simmons, *Langmuir*, **1991**, *7*, 2236.

[28] O. H. Elibol, D. Morisette, D. Akin, J. P. Denton, R. Bashir, *Applied Physics Letters*, **2003**, *83*, 4613

[29] P. J. Schubert, G. W. Neudeck, *IEEE Electron Device Letters*, **1990**, *11*, 181

[30] Z. Li, Y. Chen, X. Li, T. I. Kamins, K. Nauka, R. S. Williams, *Nano Letters*, **2004**, *4*, 245

[31] Z. Li, Y, Chen, T. I. Kamins, K., Nauka, R. S. Williams, *Applied Physics a-Materials Science & Processing*, **2005**, *80*, 1257

[32] J. T. Sheu, C.C. Chen, P.C. Huang, Y. K. Lee, M. L. Hsu, *Japanese Journal of Applied Physics Part 1-Regular Papers Brief Communications & Review Papers*, **2005**, *44*, 2864

[33] F. H. Ko, Z. H. Yeh, C.C. Chen, T. F. Liu, *Journal of Vacuum, Science & Technology B*, **2005**, *23*, 3000

[34] E. Stern, J. F. Klemic, D. A. Routenberg, P. N. Wyrembak, D. B. Turner-Evans, A. D. Hamilton, D. A. LaVan, T. M. Fahmy, M. A. Reed, *Nature*, **2007**, *445*, 519

[35] C. M. Lieber, *Mrs Bulletin*, **2003**, *28*, 486

[36] J. Janata, *Analyst*, **1994**, *119*, 2275

[37] Y. Cui, C. M. Lieber, *Science*, **2001**, *291*, 851

[38] Y. Chen, X. H. Wang, S. Erramilli, P. Mohanty, A. Kalinowski, *Applied Physics Letters*, **2006**, *89*, 22

[39] Y. Cui, Z. H. Zhong, D. L. Wang, W. U. Wang, C. M. Lieber, *Nano letters*, **2003**,

3, 149

[40] S. Jin, D. M. Whang, M. C. Mcalpin, R. S. Friedman, Y. Wu, C. M. Lieber, *Nano letters*, **2004**, *4*, 915

[41] Y. Wu, J. Xiang, C. Yang, W. U. Wang, C. M. Lieber, *Nature*, **2004**, *430*, 704

[42] G. F. Zheng, F. Patolsky, Y. Cui, W. U. Wang, C. M. Lieber, *Nature Biotechnology*, **2005**, *23*, 1294

[43] D. R. Thevenot, K. Toth, R. A. Durst, G. S. *Wilson, Biosensors & Bioelectronics*, **2001**, *16*, 121

[44] G. S. Wilson, R. Gifford, *Biosensors & Bioelectronics*, **2005**, *20*, 2388

[45] F. Patolsky, C. M. Lieber, *Materialtoday*, **2005**, 20

Chapter 3

[1] National Chiao Tung University. (NCTU) http://www.nctu.edu.tw

[2] National Nano Device Laboratories. (NDL) http://www.ndl.org.tw/web/index.html

[3] Q. Su, C. H. Schroder, W. J. Hofmann, G. Otto, R. Pichlmayr, P. Bannasch, *HAPATOLOGY*, **1998**, *27*, 1109

[4] R.B. Takkenberg, H.L. Zaaijer, R. Molenkamp, S. Menting, V. Terpstra, C.J. Weegink, M.G.W. Dijkgraaf, P.L.M. Jansen, H.W. Reesink, M.G.H.M. Beld, *J. Medical Virology*, **2009**, *81*, 988

[5] MDBio, Inc. http://www.mdbio.com.tw/

[6] TB Tomasi, Annual review of medicine, 1977, 28, 453

[7] GJ Mizejewski, Experimental biology and medicine, 2001, 226, 377

[8] ME Harper, American journal of human genetics, 1983, 35, 565

[9] Entrez Gene: AFP.

http://www.ncbi.nlm.nih.gov/sites/entrez?Db=gene&Cmd=ShowDetailView&TermToSearch=174

Chapter 4

[1] C. Rebischung, P. Pautier, P. Morice, C. Lhomme, P. Duvillard, *Gynecol. Oncol*., **2000**, *77*, 203

[2] P. R. Nair, M. A. Alam, *Nano Letter*, **2008**, *8*, 1281

[3] A. Gray, A. W. Tam, T. J. Dull, J. Hay¯ich, J. Pintor, W. K. Carenee, A. Koyfos, *DNA*, **1987**, *6*, 283

[4] E. Lamas, L. B. Bail, O. Boucher, C. Heusset, C. Brechet, *Falk Symposium*, **1989**, *55*, 45

[5] J. Scott, J. Cowell, M. E. Robertson, L. M. Prestley, R. Wadey, B. Mopkins, J. Printchard, *Nature*, **1985**, *317*, 260

[6] Y. I. Lee, S. Lee, Y. Lee, Y. S. Bong, S. W. Hyun, Y. D. Yoo, S. J. Kim, Y. W. Kim, H. R. Poo, *Oncogene*, **1998**, *16*, 2367

[7] T. B. Tomasi, Annual review of medicine, 1977, 28, 453

[8]G. J. Mizejewski, Experimental biology and medicine. 2001, 226, 377

[9] D. Ball, E. Rose, E. Alpert, Am. J. Med. Sci., 1992, 303, 157

[10] P. Sizaret,N. Martel,A. Tuyns,S. Reynaud, Digestion, 1977, 15, 97

[11] M. E. Blohm,D. Vesterling-Hörner,G. Calaminus, U. Göbel, Pediatric hematology and oncology, 1998, 15, 135

[12]K. Ohama,H. Nagase,K. Ogino, official journal of Austrian Association of Pediatric Surgery, 1997, 7, 267

[13] P. L. Lee, M. H. Chang, D. S. Chen, C. Y Lee, J. Pediatr. Gastroenterol. Nutr., 1989, 8, 19.

[14] J. I. Blair, R. Carachi, R. Gupta, F. G. Sim, E. J. McAllister, R. Weston, Arch. Dis. Child., 1987, 62, 362

[15] D. Bader, A. Riskin, O. Vafsi, Clin. Chim. Acta, 2004, 349, 15.

[16] J. T. Wu,T. Roan, J. A. Knight, Mizejewski GJ, Porter I. Alfa-Fetoprotein and Congenital Disorders, 1985, 111

[17] R. N.Pradeep, A. A. Muhammad, Nano letter, 2008, 8, 1281

[18] R. G. Wilson, P. K. Vasudev, *SOS/SOITechnology Workshop*, **1988**, 50